AIKATERINI GRATSIA

SCHOOL OF MECHANICAL ENGINEERING

Decentralized leader-follower formation control within obstacle cluttered environments under field of view constraints

Section: Mechanical Design & Automatic Control

Supervisor: Konstantinos Kyriakopoulos, Professor NTUA

Athens, June 2021

Preface

First of all, I am grateful to the Professor of School of Mechanical Engineering, Konstantinos Kyriakopoulos, for giving me the opportunity to work on this very interesting project.

I would also like to thank the Post-Doc Associate, Charalampos Bechlioulis for his guidance and his assistance during the elaboration of diploma thesis. His invaluable help was the key to the successful completion of this project and I am very happy to have had the opportunity to work with him.

Finally, I would like to thank my family for their support and their encouragement throughout my studies.

<u>Υπεύθυνη δήλωση</u> για λογοκλοπή και για κλοπή πνευματικής ιδιοκτησίας:

Έχω διαβάσει και κατανοήσει τους κανόνες για τη λογοκλοπή και τον τρόπο σωστής αναφοράς των πηγών που περιέχονται στον οδηγό συγγραφής Διπλωματικών Εργασιών. Δηλώνω ότι, από όσα γνωρίζω, το περιεχόμενο της παρούσας Διπλωματικής Εργασίας είναι προϊόν δικής μου εργασίας και υπάρχουν αναφορές σε όλες τις πηγές που χρησιμοποίησα.

Οι απόψεις και τα συμπεράσματα που περιέχονται σε αυτή τη Διπλωματική εργασία είναι του συγγραφέα και δεν πρέπει να ερμηνευθεί ότι αντιπροσωπεύουν τις επίσημες θέσεις της Σχολής Μηχανολόγων Μηχανικών ή του Εθνικού Μετσόβιου Πολυτεχνείου.

Ονοματεπώνυμο

Αικατερίνη Γρατσία

Σύνοψη

Η μελέτη των συστημάτων πολλαπλών ρομπότ αποτελεί ένα πολλά υποσχόμενο πεδίο τεχνολογίας. Ένας από τους κύριους στόχους ελέγχου αυτών των συστημάτων είναι η διατήρηση σχηματισμού. Οι προσεγγίσεις που βασίζονται σε σχηματισμούς «ρομπότ οδηγός-ρομπότ ακόλουθος» έχουν μελετηθεί εκτενώς από πολλούς ερευνητές με αποτέλεσμα να έχουν προκύψει αρκετές στρατηγικές ελέγχου. Στην παρούσα διπλωματική εργασία μελετάται το σχήμα ελέγχου της αναφοράς [1]. Η προσέγγιση αυτή αφορά ένα σύστημα μη ολονομικών, κινούμενων ρομπότ που λειτουργούν σε ένα άγνωστο περιβάλλον σε διαμόρφωση «ρομπότ οδηγός-ρομπότ ακόλουθος». Το προτεινόμενο σχήμα ελέγχου καθίσταται κατάλληλο για μία ποικιλία πρακτικών εφαρμογών λόγω της χρήσης αποκλειστικά τοπικών μετρήσεων οι οποίες λαμβάνονται από μία κάμερα που τοποθετείται στο ρομπότ ακόλουθο . Επιπλέον, λαμβάνεται υποψίν η κατάσταση απώλειας του ρομπότ οδηγού καθώς και οι περιορισμοί των εισόδων ελέγχου. Σκοπός της παρούσης διπλωματικής εργασίας αποτελεί ο έλεγχος της αποτελεσματικότητας των προτεινόμενων στρατηγικών ελέγχου σε απαιτητικά περιβάλλοντα. Για να επιτευχθεί ο συγκεκριμένος στόχος, τρεις μελέτες προσομοίωσης έχουν διεξαχθεί σε περιβάλλον MATLAB ενώ παρέχονται αποτελέσματα που αποδεικνύουν κατά πόσο αποτελεσματικό είναι το προτεινόμενο σχήμα ελέγχου σε καθένα από τα τρία περιβάλλοντα.

Abstract

The study of Multi-Robot Systems is a promising technology field and formation keeping is one of the main objectives of multirobot control. The approaches based on Leader-Follower formations have been extensively studied and many control strategies have been proposed. In this particular diploma thesis the control strategy of reference [1] is studied. This approach considers nonholonomic mobile robots operating in unknown obstacle environment in *L-F* formation. The proposed control scheme is appropriate for a variety of practical applications due to use of exclusively local state measurements obtained by a stereo camera mounted on *F* and the non-necessity of knowledge of workspace. Plus, leader-loss situation has been considered and control input constraints have explicitly been taken into account. The objective of this particular diploma thesis is to check the effectiveness of the proposed control scheme in demanding workspaces. Therefore, three simulation studies have been conducted in MATLAB environment and the results show whether the control scheme is effective in each workspace.

Nomenclature

$\{G\}$	*Global coordinate frame*	
$\{i\}$	*Body-fixed local frame* $i \in \{L, F\}$	
$\{T\}$	*Temporary coordinate frame at* t_l	
$\{V\}$	*Coordinate frame of the virtual target*	
$\mathcal{O}$	*Set of all points on obstacles in the workspace*	
p_i	*Position of robot* $i \in \{L, F\}$ *in* $\{G\}$	$[m]$
$p_{i,initial}$	*Initial position of robot* $i \in \{L, F\}$ *in* $\{G\}$	$[m]$
${}^{T}p_i$	*Position of robot* $i \in \{L, F\}$ *with respect to* $\{T\}$	$[m]$
${}^{T}p_V$	*Position of virtual target* $\{V\}$ *with respect to* $\{T\}$	$[m]$
${}^{V}p_F$	*Position of F with respect to* $\{V\}$	$[m]$
p'	*Position of the nearest obstacle with respect to* $\{G\}$	$[m]$
θ_i	*Heading angle of robot* $i \in \{L, F\}$ *in* $\{G\}$	$[rad]$
$\theta_{i,initial}$	*Initial heading angle of robot* $i \in \{L, F\}$ *in* $\{G\}$	$[rad]$
${}^{T}\theta_i$	*Heading angle of robot* $i \in \{L, F\}$ *with respect to* $\{T\}$	$[rad]$
${}^{T}\theta_V$	*Heading angle of virtual target* $\{V\}$ *with respect to* $\{T\}$	$[rad]$
${}^{V}\theta_F$	*Heading angle of F with respect to* $\{V\}$	$[rad]$
u_i	*Linear velocity of robot* $i \in \{L, F\}$	$[m/s]$
$\bar{u}_L$	*Bound of Leader's linear velocity*	$[m/s]$
$\bar{u}_F$	*Bound of Follower's linear velocity*	$[m/s]$
$u_{F,t}$	*Leader tracking part of control input* u_F	$[m/s]$
$u_{F,a}$	*Obstacle avoidance part of control input* u_F	$[m/s]$
$u_{F,p}$	*Path following part of control input* u_F	$[m/s]$
u_{avoid}	*Positive constant linear velocity*	$[m/s]$
u_{follow}	*Positive constant linear velocity*	$[m/s]$

ω_i	*Angular velocity of robot* $i \in \{L, F\}$	$[rad/s]$
$\overline{\omega}_L$	*Bound of Leader's angular velocity*	$[rad/s]$
$\overline{\omega}_F$	*Bound of Follower's angular velocity*	$[rad/s]$
$\omega_{F,t}$	*Leader tracking part of control input* ω_F	$[rad/s]$
$\omega_{F,\alpha}$	*Obstacle avoidance part of control input* ω_F	$[rad/s]$
$\omega_{F,p}$	*Obstacle avoidance part of control input* ω_F	$[rad/s]$
$\dot{u}_i$	*Linear acceleration of robot* $i \in \{L, F\}$	$[m/s^2]$
$R(\theta_i)$	*Rotation matrix of robot* $i \in \{L, F\}$	
ρ	*Distance between L & F with respect to* $\{F\}$	$[m]$
ρ'	*Relative position of the nearest obstacle with respect to* $\{F\}$	$[m]$
ρ_{min}	*Maximum of* d_{min} *and* d_{safe}	$[m]$
ρ_{max}	*Maximum detection range*	$[m]$
ρ_o	*Minimum distance between F and obstacles*	$[m]$
$\rho_{o,safe}$	*Safe distance for obstacle avoidance*	$[m]$
$\rho_{o,sen}$	*Sensitive range for obstacle avoidance*	$[m]$
ρ_d	*Desired distance between L & F*	$[m]$
d_{min}	*Minimum detection range*	$[m]$
d_{max}	*Maximum detection range*	$[m]$
d_{safe}	*Safe distance*	$[m]$
α	*Bearing angle of L with respect to* $\{F\}$	$[rad]$
α_{min}	*Minimum angle of FOV*	$[rad]$
α_{max}	*Maximum angle of FOV*	$[rad]$
α_o	*Bearing angle of the nearest obstacle measured in* $\{F\}$	$[rad]$
α_d	*Desired bearing angle of L with respect to* $\{F\}$	$[rad]$
α_{od}	*Critical bearing angle*	$[rad]$

t_l	*Time instant when L was lost*	$[s]$
t_{span}	*Time span of the simulation*	$[s]$
$B_\rho(\rho)$	*Bounded barrier function*	
$B_\alpha(\alpha)$	*Bounded barrier function*	
$B_{\alpha_o}(\alpha_o)$	*Bounded barrier function*	
β_ρ	*Design parameter*	
β_α	*Design parameter*	
β_{α_o}	*Design parameter*	
β_δ	*Positive design parameter*	
k_ρ	*Positive constant parameter*	
k_α	*Positive constant parameter*	
k_{α_o}	*Positive design parameter*	
k_1	*Positive constant parameter*	
k_2	*Positive constant parameter*	
γ	*Positive constant parameter*	
δ_ρ	*Positive constant parameter*	
δ_α	*Positive constant parameter*	
δ	*Expected transient maneuver*	
θ_δ	*Positive design parameter*	
l	*Arc length parameter*	

Subscripts

MRS	Multi-Robot systems
L	Leader
F	Follower
LOS	Line of sight
FOV	Field of view
R_{TF}	Front transition region

R_{TB}	Back transition region
R_{SF}	Front safe region
R_{SB}	Back safe region

Table of Contents

1. Introduction

1.1 Introduction in Multi-Robot Systems

Multi-Robot System (MRS) is considered a collection of two or more autonomous mobile robots which can cooperate and communicate with each other to accomplish certain tasks [2]. MRS is, nowadays, an important research area and have wide applications in almost every technological field. Coordinated tracking, emergency response and rescue, sensitive area surveillance, homecare, unknown environment exploration, natural resource monitoring, parallel and simultaneous transportation of vehicles, indoor and outdoor industrial operations such as fault diagnosis and repair, delivery of payloads and warehouse systems are just some of many applications of multi-robot systems.

A classification of MRS is presented in reference [3]. This categorization is based on four principal levels: cooperation, knowledge, coordination and organization. At the cooperation level the robots that operate together to perform a global task are characterized as cooperative and are differentiated from those that are non-cooperative. At the knowledge level robots are distinguished as aware and unaware. Aware robots have some information for the other agents of the system, while unaware robots perform their task autonomously. In the third level this specific classification includes these thee subcategories: strongly coordinated robots that perform their actions taking into account the actions of other agents, weakly coordinated and not coordinated. Finally, in the fourth level of the hierarchical structure, the categorization criterion concerns the decision system within the MRS. Thus; there are strongly centralized MRS, weakly centralized MRS and distributed MRS where every component is completely autonomous. In a centralized MRS there is an agent called leader (*L*) which provides information to other agents called followers (*F*) in order to accomplish the particular task. The above classification is presented in Figure 1: MRS taxonomy [3].

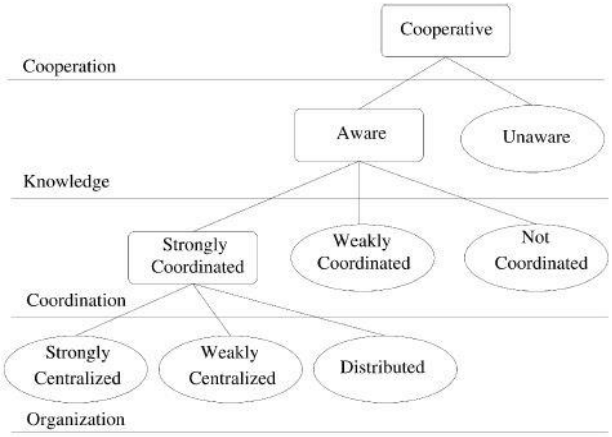

Figure 1: MRS taxonomy [3]

1.2 Formation Control Approaches

One of the fundamental goals of multirobot control is to maintain formation. Consequently, this subject has been thoroughly investigated in past years and many formation control approaches have emerged. These control schemes may be classified on many criteria.

The first categorization is based on whether or not desired formations are time-varying [4]. Thus; there are formation producing problems and formation tracking problems. In formation producing problems the objective of agents is to achieve a given desired formation shape. Matrix and Lyapunov theory, graph rigidity and receding based approach have been used to solve these problems. Furthermore, in formation tracking problems, the agents are controlled to track reference trajectories. These problems have been addressed through mainly matrix and Lyapunov theory and potential functions.

According to [4], [5] and [6] formation control schemes have been classified into behavioral, virtual and *L-F* structure approaches. In behavioral approach, desired behaviors like cohesion, collision avoidance and obstacle avoidance are specified for robots and amorphous formation control is achieved. Additionally, in virtual structure approach, the formation of agents is defined as a single object, called a virtual structure. The desired trajectories of the robots are determined from that of the virtual structure. Lastly, in *L-F* approach at least one agent, defined as a leader (*L*), tracks a given, desired trajectory, while the other agents, act as followers (*F*), track the position of the *L* with some prescribed offsets. Among the above approaches, *L-F* is simpler and more applicable. Therefore, *L-F* is preferable in most cases.

1.3 Literature Review

In practical applications the vast majority of the existing *L-F* approaches are subject to certain limitations. Sensor limitations, obstacle and interrobot collision avoidance in unknown obstacle environments, communication-free environment, unavailability of global state measurements, control input constraints and leader-loss situation are just a few of the many additional constraints.

First of all, [7] addresses the cooperative motion coordination of *L-F* formations of nonholonomic mobile robots under visibility and communication constraints in known obstacle environments. In this reference, a state feedback control scheme for *F* based on dipolar vector fields is proposed. In addition to this, a hybrid feedback motion plan has been designed for *L*, which guarantees obstacle avoidance for both robots given the cell decomposition of the free space. It is assumed that *L* ensures obstacle avoidance for both robots while navigating toward a goal configuration and *F* guarantees visibility maintenance with *L* and intervehicle collision avoidance. Plus, the upper bounds of the velocities of *L* ($\overline{u}_L, \overline{\omega}_L$) are considered known to *F* and visual detection is considered

reliable. The proposed algorithms do not require information exchange among robots, but are instead based on information locally available to each agent. Moreover, these control schemes are designed without the use of velocity measurements of mobile robots. However, the proposed control scheme is applied only in known polygonal obstacle environments and the algorithms cannot be implemented in environments that *F* cannot always maintain its visibility with *L*. Furthermore, as the number of robots grows, the turning radius of the *L* must be increased and a wider path is required. Another issue is concerned is that the tracking error from a target relative position is not guaranteed to converge to zero and the estimation of error bound is difficult especially in the case of multiple followers. If tracking error is large, connectivity maintenance and collision avoidance might not be achieved.

In [8], the problem of cooperative control design for nonlinear multi-agent systems is addressed. More specifically, the proposed control strategy ensures that a group of agents reaches a desired formation which is dependent on time-varying parameters. Initially, a control strategy was designed to stabilize the multi-agent system to a circular motion tracking. Next, a new framework relied on affine transformations was presented to extend previous results to more complex time dependent formations. Additionally, both control laws are synthesized by a cooperative term to distribute the agents uniformly along the desired formation. This study was created under the assumption that the time-varying references which define the parameters of the formation are known to all vehicles. Despite the fact that the proposed control law can be implemented in larger class formations not only circular and that the agents can be distributed uniformly along the formation in a collaborative manner, the use of global measurements and the absence of obstacle avoidance algorithm make this particular control scheme unsuitable for practical applications. Plus, there are no experimental results to demonstrate the effectiveness of this proposed control method.

The authors in [9] report a trajectory tracking control scheme for nonholonomic unicycle vehicles. The proposed control laws guarantee obstacle and intervehicle collision avoidance under limited communication at each time instant. To solve this problem, a trajectory tracking control strategy has been designed using a bounded input-output feedback linearization control law and analytical bounds on the vehicle's velocity and acceleration have been provided. The stability of internal dynamics has also been proved. Then, the tracking control law has been combined with a collision avoidance algorithm which has been designed to deal with obstacle detection errors and limited communication. Strategies for non-cooperative and cooperative cases have been developed as well. In this reference has been considered that a vehicle is able to detect the position of another vehicle or obstacle either via the use of on-board localization sensors or via the broadcast of position information among agents, whenever the latter is within the bounded sensing range of the first vehicle. Moreover, it has been assumed that the localization process among agents is subjected to sensing uncertainties. Mathematically the measurement error is considered to be bounded by some constant.

Furthermore, the radius of the avoidance region is chosen as a specification. For safety reasons, in real applications the radius is larger than the robot's radius. In addition to this, the collision avoidance control is computed by taking the distance of the first vehicle to centroid of the second vehicle. Therefore, the maximum velocity of the centroid should be taken into account and not the frontal reference point. Even though the final synthesized control law is not computationally complex, in the simulations and experiments only point and disk obstacles were considered which is unrealistic since in most practical applications the environment is unstructured. Another issue is concerned is the absence of controllability of each vehicle's orientation. Some applications require tight control of robots' orientation for proper use of sensors and other actuators.

The problem of flocking and shape-orientation control of multi-agents with inter-agent and obstacle collision avoidance has been addressed in [10]. In this reference, multiple algorithms and strategies are designed to modify the shape of the formation with aim to avoid collision with obstacles. This research is based on the assumption that the trajectory is known to only one of the agents, namely the leader of the formation and the agents can detect whether an obstacle is convex or nonconvex. Apart from that, the trajectory of *L* is planned and does not intersect with any obstacle. Moreover, all obstacles considered in this brief are assumed to be of finite extent and *L* has a directed path from all *F* at each time instant. The main contribution of this particular study is that with the proposed collision avoidance techniques the formation of the agents change size and orientation to go through a narrow passage and to avoid collision with a stationery or moving nonconvex obstacle although the existing size and orientation of formation does not allow it. However, the validity of the proposed method has not been well supported by experimental results and acceleration and turning rate constraints for the agents have not been considered. Plus, this brief is based on the assumption that each agent knows the relative position of its neighbor. In practical applications each robot may not be able to detect another agent due to camera's or sensors' limitations.

Reference [11] considers the control of a group of agents in order to track a desired trajectory and maintain a given formation in known constrained space simultaneously. The proposed control scheme is based on artificial potential field method. A modeling approach of spatial constraints in known constrained space has been designed. A Dirac delta function has also been introduced regarding to the environment's constraints. Furthermore, an optimization algorithm minimizes the formation time cost. Additionally, the stability of the multi-agent system has been studied based on Lyapunov theory. Despite the fact that rapid obstacle avoidance is achieved, this method is based on global position measurements. Therefore the proposed control scheme is not applicable for situations where only local state measurements are available. Yet there are no experimental results to validate this method's effectiveness.

The authors of [12] have presented a formation tracking controller of nonholonomic mobile robots using feedback information from a perspective camera instead of direct

position measurements. To deal with the absence of accurate position measurements, a formation controller has been designed that uses estimated relative positions, which are generated by an adaptive observer. It is assumed that each robot in the formation can directly measure its orientation θ_i and its linear and angular velocities u_i and ω_i. Even though vision sensors provide sufficient information for online estimation of the relative position, communication delays and obstacle avoidance have not been considered.

Reference [13] focuses on the problem of vision-based *L-F* formation control of mobile robots. A new real-time observer was developed to estimate the unknown camera parameters and the coefficients of the plane where the feature point moves relative to the camera frame. Additionally, the Lyapunov method was introduced to prove the stability of the closed-loop system, where it was shown that the convergence of the image error is guaranteed. Although the design and implementation of the new adaptive image-based controller is independent of leader's velocity, this method has high computational complexity. More specifically, the dynamic controller along with an image-based filter and a nonlinear observer require many complex calculations. Moreover, same as [12], sufficient information for online estimation of the relative position has been provided by vision sensors and obstacle avoidance has not been considered.

The authors of [14] have introduced a nonlinear control scheme for finite time tracking of a moving target using nonholonomic vehicles, where the distance and bearing angle of the target with respect to the velocities are constrained. A new barrier Lyapunov function was proposed to characterize non-symmetric distance and bearing angle constraints and to complement the control scheme. Despite the fact that the proposed method only employed relative position measurements with respect to the local frame attached on the vehicle without any other information required, collision avoidance has not been considered and no experimental results have been provided. Additionally, it has been proven that the tracking errors will converge to the neighborhood of zero in finite time. However, the value of the barrier function employed approaches infinity when the constraints are close to being violated, resulting in unbounded control inputs.

In [15], a multi-region control scheme has been proposed for a formation of nonholonomic vehicles to track a reference trajectory, avoid collisions and preserve network connectivity in unknown obstacle environments simultaneously. The multi-region control scheme has solved this multi-objective control problem by prioritizing different objectives in different regions. Also, potential and transition functions have been introduced to design the control laws that are necessary for robots' navigation in obstacle environments. This method is applied under the assumptions that all vehicles have equal communication and actuation capabilities and that the communication links among the vehicles follow a homogenous protocol model. In this particular model two vehicles can communicate if there are within a specified maximum communication range and cannot communicate if there are outside of that. Moreover, each vehicle is equipped with a laser rangefinder and wireless communication devices. Although the proposed

control strategy can deal with a multi-objective control problem with conflict objectives and is computationally simple, this control scheme is based on global position measurements and is not applicable for situations where only local state measurements are available. Plus, the reference trajectory and the configuration are dependent from the task and should be generated by a high-level controller.

The authors in [16] have presented *L-F* formations tracking control schemes for nonholonomic mobile robots with onboard perspective cameras without using both position and velocity measurements. It is assumed that each *F* is equipped with an onboard perspective camera which provides the necessary information for the design of formation controllers and image coordinates are used to model the *L-F* kinematics. In order to avoid the use of velocity measurements of mobile robots adaptive observers have been designed to estimate the Leader's linear velocity. Moreover, Lyapunov theory is used to analyze the stability of the closed-loop observer-controller system. However, image information from the follower's perspective onboard camera is necessary for this method's implementation. If the visibility of *L* cannot be constantly maintained, the proposed control scheme cannot be applied. Besides that, this method is computationally complex. More specifically, the velocity of *L* has to be estimated online and the relative angle has been computed using homography-based technique.

Reference [17] is a successful attempt to address the problem of moving a group of robots as a whole to a target area. A control method is proposed for *L-F* tracking in obstacle environments while preserving sensing network connectivity without communication between the robots. Collision avoidance and the fact that input constraints are not violated are ensured by the control inputs. This study is based on the following two assumptions; Only *L* knows the path to the target area and each robot in the group is subject to limited sensing and communication range. The direction of the robots' movement is decided using an artificial potential function. Subsequently, the amount of movement is determined considering the network connectivity and many additional constraints in order to achieve LOS (line of sight) visibility preservation, obstacle and interrobot collision avoidance. A methodology was also introduced to change network connectivity by deactivating some sensing links to pass the robots through narrow spaces without getting stuck ore increasing active links to keep the group cohesive in free spaces. Nevertheless, this *L-F* approach is only applied when LOS is preserved, but the obstacle avoidance behavior may break distance and bearing angle constraints resulting in loss detection of *L.* Plus, robots may get stuck in a corner even if sensing links are properly deactivated depending on the width of the path.

In [18] the *L-F* formation control problem for nonholonomic vehicles is addressed. *L* and *F* are equipped with onboard sensors to provide only bearing measurements to each other. The linear velocity of leader u_L is bounded and differentiable. The linear acceleration of leader $\dot{u}_L$ and the heading angular velocity ω_L are bounded too. An estimator has been designed to determine the relative position in its local coordinate frame using only

bearing measurements. Then, a control law has been developed for *F.* It has been proved that the estimation error converges to zero and that the closed loop system is stable if certain conditions are satisfied. Although the case of multiple followers has been considered and the proposed estimator has been developed based on nonlinear formation kinematics without linearization, there are no experimental results to demonstrate the effectiveness of the proposed control scheme. Moreover, obstacle avoidance has not been considered.

In [19] the problem of *L-F* tracking control of mobile robots based solely on onboard monocular cameras that subject to visibility constraints is presented. This study is based on two main assumptions; the velocity of *L* cannot be measured but is bounded and the feature point of *L* is initially within the FOV (field of view) of camera. An error transformation with certain specifications and *L-F* visual kinematics in the image plane has been developed. Next, in order to ensure the stability of the closed loop system an adaptive control strategy has been proposed which estimates online the inverse height between the optical center of the camera and the feature point attached to *L.* It should be noted that the presented control strategy is computationally simple as it does not require the estimation of leader's relative position. Even though the proposed control scheme relies on onboard visual sensors without communication as it does not depend on relative position measurements between the robots or the velocity of leader, intervehicle and obstacle collision avoidance have not been considered. Additionally, the cases in which the feature images are temporarily lost have not been studied.

The authors of [20] have proposed a control strategy for trajectory tracking in unknown obstacle environments using only the measurements of *F*. During the whole control task, the linear and angular velocities of L are unknown, but the upper bound of linear velocity can be obtained by *F.* Moreover, it is assumed that the goal position remains constant inside the obstacle avoidance region. The methodology of this reference is presented as follows. Initially, the trajectory tracking control problem has been analyzed based on information provided by the onboard sensors of *F.* Then, an obstacle avoidance algorithm has been proposed using a rotating matrix based approach. Furthermore, a dynamic surface control scheme has been designed and a low-pass filter has been introduces in order to decrease the communication cost. Apart from that, the disturbance rejection of the closed-loop system in case of unknown input has been studied. It should be noted that the proposed obstacle avoidance algorithm can discard the local minima and solve the obstacle avoidance problem in polar coordinates. However, leader loss situation and the case of multi-vehicle system have not been considered.

Reference [21] addresses the problem of adaptive output-feedback formation tracking control for networked uncertain nonholonomic mobile robots with different limited communication distances and simultaneously manages connectivity preservation and obstacle avoidance. The velocities of robots are unknown and are estimated based on the output of the systems. First of all, the authors of [21] have presented the specifications,

the requirements and the assumptions of the problem. Next, an adaptive observer based on neural networks has been proposed. Additionally, a nonlinear error transformation design strategy has been developed that can ensure both the maintenance of initial connectivity and the obstacle avoidance. Then, Lyapunov theory has been used to verify the stability of the proposed closed-loop system. It is important that the unknown nonlinear term of the system was estimated by only one neural network. For this reason, the unknown nonlinearity which was developed in the process of controller design does not need an additional neural network. Even though, the proposed method has low installation and maintenance cost, high flexibility and easy interoperability, there are no experimental results to demonstrate the effectiveness of the proposed algorithm. Plus, if the network resources are limited in the communication channel, the network formation control scheme may be impractical.

In the aforementioned contributions sensor limitations, obstacle and interrobot collision avoidance in unknown obstacle environments as well as leader-loss situation have not always been taken into account. It should be noted that in practical applications a stereo camera is generally employed for *F* in order to detect *L.* However, stereo cameras have minimum and maximum distance requirements and specific FOV. Moreover, if these constraints are defined with respect to the global coordinate frame cannot be used to describe stereo camera limitations. Another important issue is obstacle and intervehicle collision avoidance. Provided that safety must always be considered, prior knowledge of obstacle environment is unrealistic for practical applications. Furthermore, leader-loss situation has also not been addressed. The obstacle avoidance behavior may break the camera's constraints resulting in the loss of *L*. Loss of *L* could also be caused from environmental interference and blurring. In this diploma thesis is studied reference [1]. In this particular brief, the tracking control law that has been proposed takes sensor and control input limitations explicitly into account and the safety in unknown obstacle environment is ensured by a multiregional obstacle avoidance algorithm. Besides that, there are experiments to demonstrate the effectiveness of the proposed algorithms. Lastly, the leader-loss situation was highlighted and a control strategy has been provided.

1.4 Thesis Scope

As shown above, *L-F* structure approach is preferred for maintaining a specific formation in most practical applications of MRS. Reference [1] addresses *L-F* problem in unknown obstacle environment and considers sensor and control input limitations as well as leader loss situation. Based on reference [1] the scope of this diploma thesis is to cover the following topics:

- Is the proposed control strategy effective in an environment with many polygonal obstacles?
- Is the effectiveness of the proposed control scheme demonstrated in the case of multiple followers?
- Is the effectiveness of the proposed control algorithms validated in a workspace with rooms and narrow passages?
- How effective is the proposed control scheme in a workspace similar to zigzag with sharp corners and many non-convex obstacles?

2. Problem Description

The control strategy that is studied in this particular diploma thesis considers a MRS of two differential-drive wheeled mobile robots [1]. These robots move in a two-dimensional environment with unknown obstacles using vision-based *L-F* techniques. One of the robots called *L* moves autonomously in the workspace, while the other one, defined as *F,* is responsible for tracking *L* and achieving obstacle and intervehicle collision avoidance subject to sensor limitations and control input constraints. The robots cannot communicate with each other and only local state measurements are available. The proposed control techniques can be applied to a formation with more than two robots.

2.1 Nonholonomic Constraints

The motions of a multibody mobile robot are constrained by kinematic constraints involving the velocity [22]. Nonholonomic equality constraints are caused by the contacts between the wheels and the ground. These contacts are considered to be pure rolling contacts between rigid bodies. They express the fact that the relative velocity of two points in contact is zero. It is proved that these constraints are nonintegrable. They make the dimension of the space of admissible velocities smaller than the dimension of the robot's configuration space. Although they reduce the local mobility of the robot, they do not affect the robot's ability to move in random paths with suitable movements.

2.2 Kinematics of Differential Drive Robot

2.2.1 Motion Model

The global coordinate frame is defined as $\{G\} = \{\vec{x}_G, \vec{y}_G\}$ and robot's i body-fixed local frame is defined as $\{i\} = \{\vec{x}_i, \vec{y}_i\}$ where $i \in \{L, F\}$. The position $p_i = [x_i, y_i]^T \in \mathbb{R}^2$ and the heading angle θ_i of robot i are expressed in global coordinate frame. The relationship between the two frames is presented using basic transformation matrix as follows:

$$\begin{aligned} \dot{o}_i &= R(\theta_i)\dot{o}_G \\ &= R(\theta_i)[\dot{x}_i \quad \dot{y}_i \quad \dot{\theta}_i]^T \end{aligned} \tag{2.1}$$

where,

$$R(\theta_i) = \begin{bmatrix} cos\theta_i & sin\theta_i & 0 \\ -sin\theta_i & cos\theta_i & 0 \\ 0 & 0 & 1 \end{bmatrix} \tag{2.2}$$

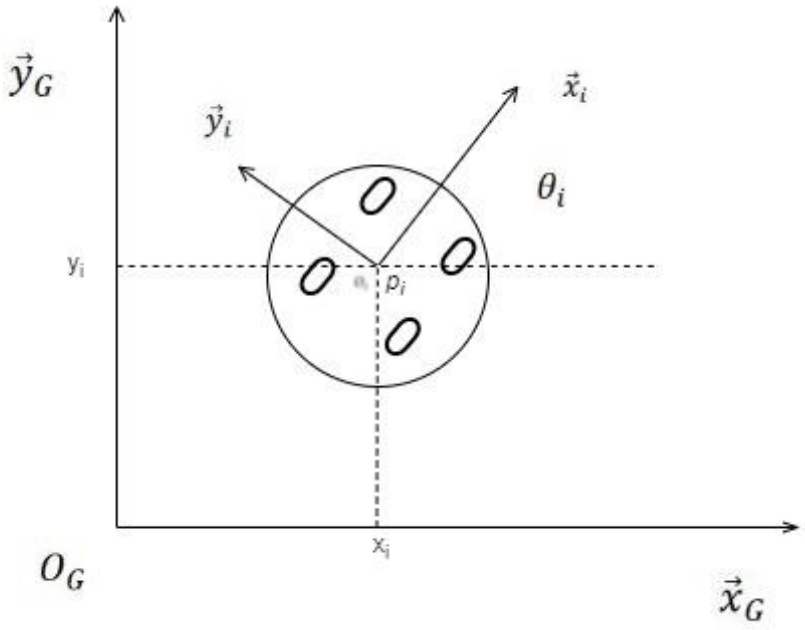

Figure 2: Representation of robot *i* with respect to the global coordinate frame

Each individual wheel contributes to the robot's motion and at the same time, imposes constraints on the movement of the robot [23]. For instance, it is assumed that the wheels of the robot do not slide. This restriction is expressed by a nonholonomic constraint as follows.

$$\dot{x}_i sin\theta_i - \dot{y}_i cos\theta_i = 0 \tag{2.3}$$

It should be noted that the actual robot motion commands are the angular velocities of the right and left wheel, rather than the robot driving and steering velocities u_i and ω_i.

2.2.2 Kinematic Equations

The kinematic model of the robots is given below.

$$\begin{aligned} \dot{x}_i &= u_i cos\theta_i \\ \dot{y}_i &= u_i sin\theta_i \\ \dot{\theta}_i &= \omega_i \end{aligned} \tag{2.4}$$

where u_i and ω_i are the linear and angular velocities of robot i with respect to its body-fixed local frame $\{i\} = \{\vec{x}_i, \vec{y}_i\}$.

2.3 Modeling of the L-F Pair

A stereo camera is mounted on *F* to detect the relative position including distance and bearing angle of *L* with respect to {*F*}.

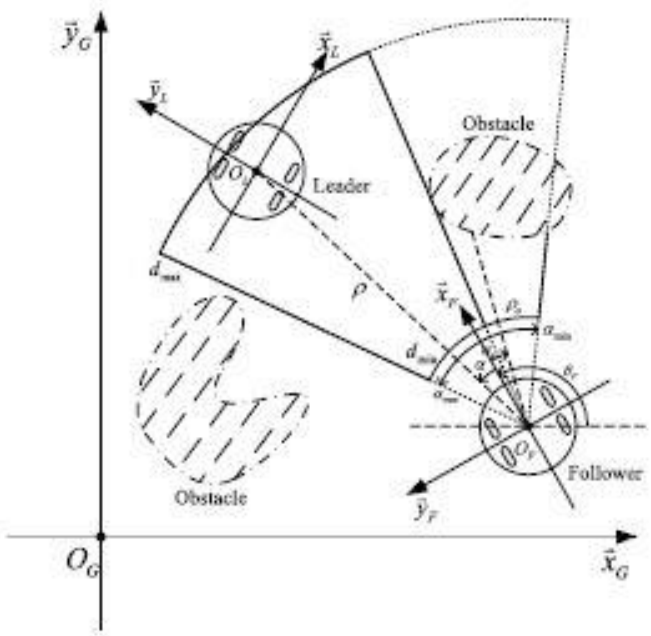

Figure 3: The relative position relationship between *L* & *F* [1]

Moreover, the distance ρ between *L* and *F* as well as the bearing angle α of *L* with respect to {*F*} using polar coordinates are defined as

$$\rho = \|p_L - p_F\|_2 \tag{2.5}$$

$$\alpha = arctan2(\tilde{y}_L, \tilde{x}_L) \tag{2.6}$$

where $(\tilde{x}_L, \tilde{y}_L)$ is the Cartesian coordinates of *L* with respect to {*F*}

$$\begin{bmatrix}\tilde{x}_L \\ \tilde{y}_L\end{bmatrix} = \begin{bmatrix} cos\theta_F & sin\theta_F \\ -sin\theta_F & cos\theta_F \end{bmatrix} \begin{bmatrix} x_L - x_F \\ y_L - y_F \end{bmatrix} \tag{2.7}$$

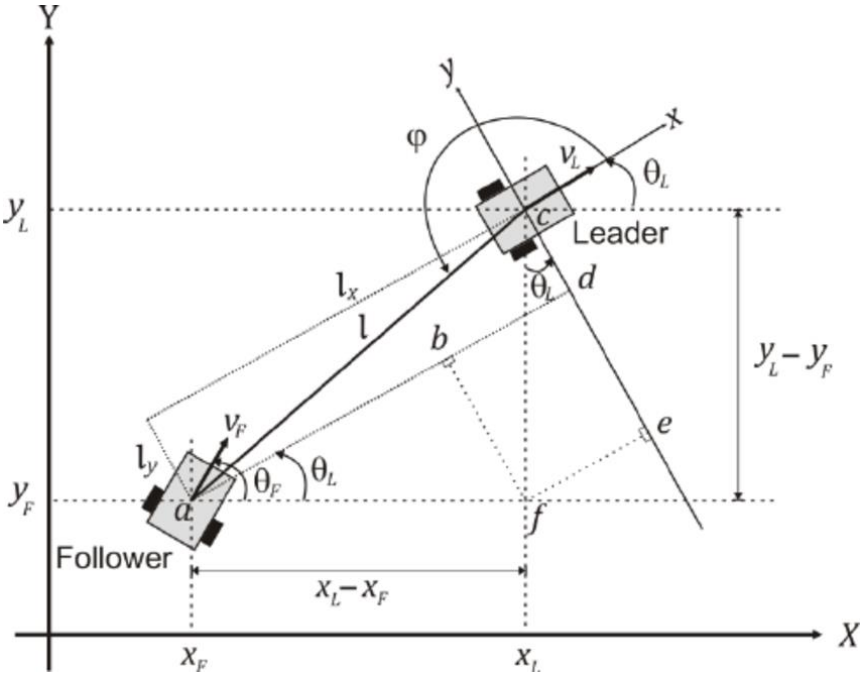

Figure 4: Cartesian coordinates of L with respect to {*F*} [24]

As mentioned above ρ and α can be obtained by the stereo camera. With some simple calculations the dynamics of ρ and α can be given as:

$$\dot{\rho} = -u_F cos\alpha + u_L \cos(\theta_L - \theta_F - \alpha) \tag{2.8}$$

$$\dot{\alpha} = -\omega_F - \frac{u_F}{\rho} sin\alpha + \frac{u_L}{\rho} sin(\theta_L - \theta_F - \alpha) \tag{2.9}$$

According to the physical meanings $\rho \in (0, +\infty)$ and $\alpha \in (-\pi, \pi]$

2.4 Modeling of the System Constraints

The stereo camera has specific FOV and limited depth range. Thus, to avoid loss of detection ρ must be smaller than the maximum detection range d_{max} and larger than the minimum detection range d_{min}. Moreover, to achieve intervehicle collision avoidance ρ must be larger than the safe distance d_{safe}. The safe distance is determined by taking into account certain parameters such as the robot's radius and the exact position of the stereo camera. Similarly, α must be larger than the minimum angle of FOV α_{min} and smaller than the maximum angle of FOV α_{max}. Consequently, the constraints on ρ and α can be defined as follows:

$$\rho \in [\rho_{min}, \rho_{max}] \tag{2.10}$$

$$\alpha \in [\alpha_{min}, \alpha_{max}] \tag{2.11}$$

where

$$\rho_{min} = \max\{d_{min},\ d_{safe}\} \tag{2.12}$$

$$\rho_{max} = \ d_{max} \tag{2.13}$$

Therefore, $\rho_{min}, \rho_{max}, \alpha_{min}$ and α_{max} are constant parameters and are selected as specifications with priority in safety. Furthermore, the requirements of the specific application and the sensor limitations are explicitly taken into account.

In addition, in order to guarantee the obstacle avoidance, the local position of the obstacle, measured in {*F*} is defined. In the same way, the minimum distance between the obstacle and *F* as well as the bearing angle of obstacle measured in {*F*} are defined as ρ_o and α_o respectively. Moreover, a sufficient condition for obstacle avoidance is presented as follows

$$\rho_o \ \geq \ \rho_{o,safe} \tag{2.14}$$

where

$$\rho_o = min\|p_F - p_o\|_{2,} \forall\ p_o \ \in \ \mathcal{O} \tag{2.15}$$

The set of all the points on obstacles in the workspace is defined as $\mathcal{O}$ and $\rho_{o,safe}$ is the safe distance between *F* and obstacles. Safe distance is determined based on the requirements of the application as well as the size of the robot and must be greater than the radius of the robot. The distance ρ_o is also obtained by the stereo camera and is shown in Figure 3.

Apart from the aforementioned constraints, the linear velocity and angular velocity of both robots are bounded due to electromechanical limitations and system requirements. Consequently, the control input constraints are expessed as

$$\begin{aligned} |u_L| &\leq \ \bar{u}_L \\ |\omega_L| &\leq \ \bar{\omega}_L \\ |u_F| &\leq \ \bar{u}_F \\ |\omega_F| &\leq \ \bar{\omega}_F \end{aligned} \tag{2.16}$$

where $\bar{u}_L$ and $\bar{\omega}_L$ are the bounds of linear velocity u_L and angular velocity ω_L respectively, while $\bar{u}_F$ and $\bar{\omega}_F$ are the bounds of u_F and ω_F, respectively. Although *F* has no knowledge of the velocity of *L*, it is assumed that the bound $\bar{u}_L$ is known to *F.* Also, *F* is able to catch up with *L* if u_F is larger than u_L.

3. Methodology

This section presents the methodology for determining the control inputs at leader tracking, unknown obstacle avoidance and leader-loss situation as well as the overall procedure for conducting the three simulation studies.

3.1 Leader Tracking

In [1] a control scheme is proposed for *F* to track *L* when there are no obstacles nearby. It is proved that with this control strategy the constraints (2.14) and (2.16) will not be violated. Moreover, the distance ρ between *L* and *F* converge to a desired value ρ_d. Similarly, the bearing angle α of *L* with respect to {*F*} converges to the neighborhood of the value α_d. Intervehicle collision avoidance is also guaranteed. Next, in order to describe the constraints of ρ and α mathematically, the following bounded barrier functions are presented.

$$B_\rho(\rho) = \begin{cases} \beta_\rho \dfrac{(\rho - \rho_d)^2}{(\rho_{max} - \rho_d)^2}, & \rho_d < \rho \leq \rho_{max} \\ \beta_\rho \dfrac{(\rho - \rho_d)^2}{(\rho_d - \rho_{min})^2}, & \rho_{min} \leq \rho \leq \rho_d \end{cases} \tag{3.1}$$

$$B_\alpha(\alpha) = \begin{cases} \beta_\alpha \dfrac{(\alpha - \alpha_d)^2}{(\alpha_{max} - \alpha_d)^2}, & \alpha_d < \alpha \leq \alpha_{max} \\ \beta_\alpha \dfrac{(\alpha - \alpha_d)^2}{(\alpha_d - \alpha_{min})^2}, & \alpha_{min} \leq \alpha \leq \alpha_d \end{cases} \tag{3.2}$$

Obviously, the design parameters β_ρ and β_α satisfy the following mathematical relations

$$\beta_\rho = B_\rho(\rho_{max}) = B_\rho(\rho_{min}) \tag{3.3}$$

$$\beta_\alpha = B_\alpha(\alpha_{max}) = B_\alpha(\alpha_{min}) \tag{3.4}$$

With some straightforward calculations it is shown that $\min\left(B_\rho(\rho)\right) = 0$ at $\rho = \rho_d$ and $\max\left(B_\rho(\rho)\right) = \beta_\rho$ when $\rho = \rho_{max}$ or $\rho = \rho_{min}$ as well as B_ρ is an increasing function. Likewise for increasing function B_α: $\min\left(B_\alpha(\alpha)\right) = 0$ at $\alpha = \alpha_d$ and $\max\left(B_\alpha(\alpha)\right) = \beta_\alpha$ when $\alpha = \alpha_{max}$ or $\alpha = \alpha_{min}$.

Additionally, a control scheme for *F* to track *L* is introduced using the functions (3.1) and (3.2).

$$u_{F,t} = \frac{1}{cos\alpha}\left[k_\rho \nabla B_\rho + \bar{u}_L \tanh\left(\frac{\bar{u}_L \nabla B_\rho}{\delta_\rho}\right)\right] \tag{3.5}$$

$$\omega_{F,t} = \frac{u_F}{\rho} sin\alpha + \frac{\bar{u}_L}{\rho}\tanh\left(\frac{\bar{u}_L \nabla B_\alpha}{\rho\delta_\alpha}\right) + k_\alpha \nabla B_\alpha \tag{3.6}$$

where $k_\rho, k_\alpha, \delta_\rho$ and δ_α are positive constant parameters, ∇B_ρ and ∇B_α are the gradients of B_ρ and B_α with respect to ρ and α, respectively. Furthermore, k_ρ and k_α satisfy the

$$k_\rho \leq \frac{\bar{u}_F \xi_\rho - \bar{u}_L}{G_\rho} \tag{3.7}$$

$$k_\alpha \leq \frac{\bar{\omega}_F \rho_{min} - \bar{u}_L - \bar{u}_F \xi_\alpha}{G_\alpha \rho_{min}} \tag{3.8}$$

below conditions:

where

$$\xi_\rho = \min\{cos\alpha_{min}, cos\alpha_{max}\} \tag{3.9}$$

$$G_\rho = \max\left\{\frac{2\beta_\rho}{\rho_{max} - \rho_d}, \frac{2\beta_\rho}{\rho_d - \rho_{min}}\right\} \tag{3.10}$$

$$\xi_\alpha = \min\{sin\alpha_{min}, sin\alpha_{max}\} \tag{3.11}$$

$$G_\alpha = \max\left\{\frac{2\beta_\alpha}{\alpha_{max} - \alpha_d}, \frac{2\beta_\alpha}{\alpha_d - \alpha_{min}}\right\} \tag{3.12}$$

3.2 Unknown Obstacle Avoidance

In many practical applications, the environment information may change during operation or be unavailable. Therefore, the authors of [1] have proposed a control scheme for unknown obstacle environment. For safety reasons is important for robots to consider the nearest obstacle every time instant. In this particular algorithm *F* detects the nearest obstacle within the *FOV.* Furthermore, a set of regions is presented according to the relative position of the nearest obstacle with respect to {*F*}. These regions are front transition region R_{TF}, back transition region R_{TB}, front safe region R_{SF} and back safe region R_{SB} and are defined as

$$R_{TF} \triangleq \left\{p' | \rho_{o,safe} < \rho' \leq \rho_{o,sen}, |a'| \leq \frac{\pi}{2}\right\} \tag{3.13}$$

$$R_{TB} \triangleq \left\{p' | \rho_{o,safe} < \rho' \leq \rho_{o,sen}, |a'| > \frac{\pi}{2}\right\}$$

$$R_{SF} \triangleq \left\{p' | \rho' \leq \rho_{o,safe}, |a'| \leq \frac{\pi}{2}\right\}$$

$$R_{SB} \triangleq \left\{p' | \rho' \leq \rho_{o,safe}, |a'| > \frac{\pi}{2}\right\}$$

where

$$p' = [x', y']^T \tag{3.14}$$

$$\rho' = \|p' - p_F\|_2 \tag{3.15}$$

$$\alpha_o = atan2(\tilde{y}', \tilde{x}') \tag{3.16}$$

$$\begin{bmatrix}\tilde{x}' \\ \tilde{y}'\end{bmatrix} = \begin{bmatrix} cos\theta_F & sin\theta_F \\ -sin\theta_F & cos\theta_F \end{bmatrix} \begin{bmatrix} x' - x_F \\ y' - y_F \end{bmatrix} \tag{3.17}$$

and $\rho_{o,sen}$ and $\rho_{o,safe}$ are the sensitive and safe distance for obstacle avoidance respectively. Obviously,

$$\rho_{o,sen} > \rho_{o,safe} \tag{3.18}$$

Additionally, p' Position of the nearest obstacle with respect to $\{G\}$, ρ' is the relative position of the nearest obstacle with respect to {*F*}, α_o is the Bearing angle of the nearest obstacle measured in $\{F\}$ and $(\tilde{x}', \tilde{y}')$ are the Cartesian coordinates of the nearest obstacle with respect to $\{F\}$.

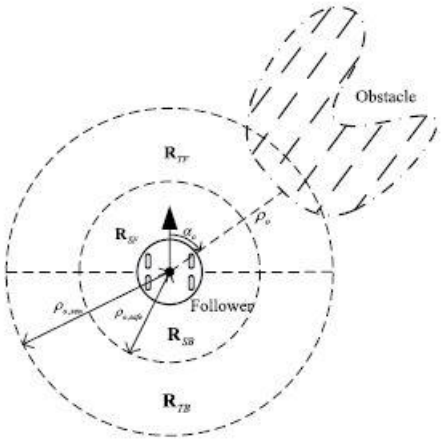

Figure 5: Diagram of obstacle avoidance [1]

In Figure 5: Diagram of obstacle avoidance [1] the relative position between *F* and the obstacle is depicted. An example is also shown where the nearest obstacle is detected in R_{TF} and the four regions are illustrated.

Next, a bounded barrier function is introduced in [1] to describe the obstacle bearing angle constraint:

$$B_{\alpha_o}(\alpha_o) = \begin{cases} \beta_{\alpha_o} \dfrac{(\alpha_o - \alpha_{od})^2}{{\alpha_{od}}^2}, 0 < \alpha_o \leq \alpha_{od} \\ \beta_{\alpha_o} \dfrac{(\alpha_o + \alpha_{od})^2}{{\alpha_{od}}^2}, -\alpha_{od} \leq \alpha_o \leq 0 \end{cases} \tag{3.19}$$

where α_o is the bearing angle of the nearest obstacle with respect to $\{F\}$, β_{α_o} is a design parameter and α_{od} is the critical bearing angle. If $\alpha_{od} = \frac{\pi}{2}$, F will move away from the obstacle with a positive u_F. However, in experiments α_{od} should be larger than $\frac{\pi}{2}$, due to friction and mechanical disturbances.

Based on aforementioned definitions, a multiregional obstacle algorithm is proposed in [1] and is presented in Table 1.

Table 1: Multiregional Obstacle Avoidance Algorithm

Input: $\boldsymbol{\rho_o, \alpha_o}$
Output: $\boldsymbol{u_F, \omega_F}$
switch **(Region where the obstacle is located)**
case $\boldsymbol{R_{TF}}$: $\boldsymbol{u_F = u_{F,t}, \omega_F = \min\{\omega_{F,t} + \omega_{F,a}, \bar{\omega}_F\}}$
case $\boldsymbol{R_{TB}}$: $\boldsymbol{u_F = u_{F,t}, \omega_F = \omega_{F,t}}$
case $\boldsymbol{R_{SF}}$: $\boldsymbol{u_F = 0, \omega_F = \omega_{F,a}}$
case $\boldsymbol{R_{SB}}$: $\boldsymbol{u_F = u_{F,a}, \omega_F = 0}$
default: $\boldsymbol{u_F = u_{F,t}, \omega_F = \omega_{F,t}}$
end switch

In this algorithm, there are two parts that compose the control input: the leader tracking part and the obstacle avoidance part. Thus, $u_{F,t}$ and $u_{F,a}$ are the linear velocities of leader tracking and obstacle avoidance respectively, as well as $\omega_{F,t}$ and $\omega_{F,a}$ are the angular velocities of leader tracking and obstacle avoidance, respectively. The leader

tracking velocities $u_{F,t}$ and $\omega_{F,t}$ are defined in equations (3.5) and (3.6) while $u_{F,a}$ and $\omega_{F,a}$ are defined as follows

$$u_{F,a} = u_{avoid} \tag{3.20}$$

$$\omega_{F,a} = k_{\alpha_o} \nabla B_{\alpha_o} \tag{3.21}$$

where u_{avoid} is a positive constant linear velocity, k_{α_o} is a positive design parameter and ∇B_{α_o} is the gradient of B_{α_o} with respect to α_o. Apart from that, the control parameters satisfy the following constraints

$$|u_{avoid}| \leq \bar{u}_F \tag{3.22}$$

$$k_{\alpha_o} \leq \frac{\bar{\omega}_F}{G_{\alpha_o}} \tag{3.23}$$

where $G_{\alpha_o} = \frac{2\beta_{\alpha_o}}{\alpha_{od}}$. As can been seen from the algorithm, when ρ_o is larger than $\rho_{o,sen}$ the obstacle is not taken into account and only leader tracking is activated. Similarly, in region R_{TB}, the obstacle is located behind *F* and does not threaten its safety. Furthermore, when the obstacle is located in front of *F* and the distance ρ_o is smaller than $\rho_{o,sen}$ and larger than $\rho_{o,safe}$, i.e. in region R_{TF}, the control input combines both leader tracking and obstacle avoidance. The linear velocity u_F achieves the leader tracking objective and remains equal to $u_{F,t}$ and the angular velocity ω_F achieves the leader tracking and obstacle avoidance objectives simultaneously. While in R_{SF}, ρ_o is smaller than $\rho_{o,safe}$. Therefore, *F* stops and rotates so that the obstacle is transferred to R_{SB}, where *F* maintains its heading angle and moves away. As can been seen, with the above multiregional algorithm, unknown obstacle avoidance is guaranteed.

3.3 Leader-Loss Reaction

The leader-loss situation is caused by motion blurring, environment interference and obstacle avoidance behavior where the distance and bearing angle constraints may be broken. Obviously, in practical applications *L* cannot maintain its visibility with *F* every time instant. For this reason, the authors of [1], in order to address this particular problem, have proposed a fault-tolerant strategy and have designed a control scheme for this situation.

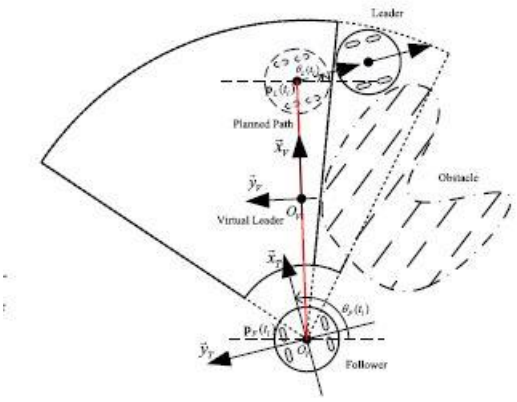

Figure 6: Leader-loss example, where *L* is occluded by an obstacle [1]

Additionally, the fault-tolerant strategy is described. In the first place, the goal state is determined. The goal state is the position and the heading angle of *L,* the last time instant that *L* was in the FOV, which is actually the last detected leader state. Then, the shortest path for *F* from the current state to the goal state needs to be found. Next, a control law is designed to move *F* along the path to the goal state as fast as possible.

Moreover, to design a fault-tolerant strategy it should be mentioned that the global coordinates and the heading angle of robots at every time instant are not available. Thus, at t_l, i.e. at time instant when *L* was lost the global states of *L* and *F* cannot be obtained. For this reason, a temporary coordinate frame $\{T\} = \{\vec{x}_T, \vec{y}_T\}$ is defined which is coincident with the local frame $\{F\}$ at t_l.

$$\{T\} = \{F\}|_{t=t_l} \tag{3.24}$$

From the aforementioned analysis, in the proposed fault-tolerant strategy the shortest path ${}^T p_V(l)$ is planned from the starting state $\left({}^T p_F(t_l), {}^T\theta_F(t_l)\right)$ to the goal state $\left({}^T p_L(t_l), {}^T\theta_L(t_l)\right)$, where l is the arc length parameter, $\left({}^T p_F(t_l), {}^T\theta_F(t_l)\right)$ and $\left({}^T p_L(t_l), {}^T\theta_L(t_l)\right)$ are the states of *F* and *L* measured at t_l with respect to $\{T\}$. A control law is also designed to drive *F* along the planned path and reach the goal as fast as possible.

The first objective of the proposed fault-tolerant strategy is to solve a shortest path plan problem. Based on [25], the shortest path takes the form of CSC. The curvature of this path is constrained. In CSC, C denotes a circular arc with minimum turning radius and S denotes a straight-line segment. The shortest path from $\left({}^T p_F(t_l), {}^T\theta_F(t_l)\right)$ to $\left({}^T p_L(t_l), {}^T\theta_L(t_l)\right)$ is simply a straight line connecting ${}^T p_F(t_l)$ and ${}^T p_L(t_l)$ given that the minimum turning radius of the robot is assumed to be zero.

Furthermore, the second objective is to design a suitable control law for driving *F* to move along the planned path to the goal point while the obstacle avoidance and control input constraints should also be guaranteed. Additionally, two parts: following path part and obstacle avoidance part compose the total control input.

The path following control input is designed according to [26]. A virtual target:

$$\{V\} = \{\vec{x}_V, \vec{y}_V\}$$

which moves along the planned path is introduced. The virtual target and the planned path are shown in Figure 6. Next, the following definitions are given:

$$^{T}p_F = [\,^{T}x_F,\ ^{T}y_F]^T \tag{3.25}$$

$$^{T}p_V = [\,^{T}x_V,\ ^{T}y_V]^T \tag{3.26}$$

$$^{V}p_F = [\,^{V}x_F,\ ^{V}y_F]^T \tag{3.27}$$

where $^{T}p_F$ is the position of *F* in $\{T\}$, $^{T}p_V$ is the position of virtual target $\{V\}$ with respect to $\{T\}$, $^{V}p_F$ is the position of *F* in $\{V\}$, $^{T}\theta_F$ is the heading angle of *F* in $\{T\}$, $^{T}\theta_V$ is the heading angle of $\{V\}$ in $\{T\}$ and $^{V}\theta_F$ is the heading angle of *F* in $\{V\}$. In addition to this, the path following error dynamics are presented as follows:

$$\begin{aligned} ^{V}\dot{x}_F &= -\dot{l} + u_{F,p} cos\,^{V}\theta_F \\ ^{V}\dot{y}_F &= u_{F,p} sin\,^{V}\theta_F \\ ^{V}\dot{\theta}_F &= \omega_{F,p} \end{aligned} \tag{3.28}$$

where

$$^{V}\theta_F = \ ^{T}\theta_F - \ ^{T}\theta_V \tag{3.29}$$

The rate of progression of the virtual target $\{V\}$ along the planned path can be derived as follows:

$$\dot{l} = u_{F,p} cos\,^{T}\theta_F + k_1\,^{V}x_F \tag{3.30}$$

where k_1 is a positive constant parameter. Apart from that, the path following control law is defined as follows

$$u_{F,p} = u_{follow} \tag{3.31}$$

$$\begin{aligned} \omega_{F,p} = \dot{\delta} - \gamma \tanh(^{V}y_F)\left[1 - tanh^2(^{V}y_F)\right] u_{F,p} \frac{sin\,^{V}\theta_F - sin\delta}{^{V}\theta_F - \delta} \\ -k_2 \tanh(^{V}\theta_F - \delta) \end{aligned} \tag{3.32}$$

where k_2 and γ are positive constant parameters. Given that *F* moves at a constant speed along the path, u_{follow} is a positive constant linear velocity. Furthermore, δ is the expected transient maneuver and is described by the following equation

$$\delta = -\theta_\delta \tanh(\beta_\delta {}^V y_F) \tag{3.33}$$

$$\dot{\delta} = -\theta_\delta \left[1 - tanh^2\left(\beta_\delta {}^V y_F\right)\right] \beta_\delta {}^V \dot{y}_F \tag{3.34}$$

where β_δ and θ_δ are positive design parameters. Moreover the following conditions are satisfied.

$$u_{follow} \leq \bar{u}_F \tag{3.35}$$

$$k_2 + \theta_\delta \beta_\delta u_{F,p} + \frac{2\sqrt{3}}{9} \gamma u_{F,p} \leq \bar{\omega}_F \tag{3.36}$$

It is also proved that ${}^V p_F$ and ${}^V \theta_F$ will converge to zero asymptotically.

Next, the algorithm of fault-tolerant strategy for Leader-Loss Situation is presented in Table 2: Fault-Tolerant Strategy for Leader-Loss Situation

Table 2: Fault-Tolerant Strategy for Leader-Loss Situation

Input: $\left({}^{T}\boldsymbol{p}_{L}(\boldsymbol{t}_{l}),\ {}^{T}\boldsymbol{\theta}_{L}(\boldsymbol{t}_{l})\right), \left({}^{T}\boldsymbol{p}_{F}(\boldsymbol{t}_{l}),\ {}^{T}\boldsymbol{\theta}_{F}(\boldsymbol{t}_{l})\right), \boldsymbol{\rho}_{o}, \boldsymbol{\alpha}_{o}$
Output: $\boldsymbol{u}_{F}, \boldsymbol{\omega}_{F}$
Plan the shortest path ${}^{T}\boldsymbol{p}_{V}(\boldsymbol{l})$ from $\left({}^{T}\boldsymbol{p}_{F}(\boldsymbol{t}_{l}),\ {}^{T}\boldsymbol{\theta}_{F}(\boldsymbol{t}_{l})\right)$ to $\left({}^{T}\boldsymbol{p}_{L}(\boldsymbol{t}_{l}),\ {}^{T}\boldsymbol{\theta}_{L}(\boldsymbol{t}_{l})\right)$
Design path following control part $\boldsymbol{u}_{F,p}$ and $\boldsymbol{\omega}_{F,p}$ to drive *F* moving along ${}^{T}\boldsymbol{p}_{V}(\boldsymbol{l})$
Design the control law $\boldsymbol{u}_{F}$ and $\boldsymbol{\omega}_{F}$
switch **(Region where the obstacle is located)**
case $\boldsymbol{R}_{TF}$: $\boldsymbol{u}_{F} = \boldsymbol{u}_{F,p}, \boldsymbol{\omega}_{F} = \mathbf{min}\{\boldsymbol{\omega}_{F,p} + \boldsymbol{\omega}_{F,a}, \bar{\boldsymbol{\omega}}_{F}\}$
case $\boldsymbol{R}_{TB}$: $\boldsymbol{u}_{F} = \boldsymbol{u}_{F,p}, \boldsymbol{\omega}_{F} = \boldsymbol{\omega}_{F,p}$
case $\boldsymbol{R}_{SF}$: $\boldsymbol{u}_{F} = \mathbf{0}, \boldsymbol{\omega}_{F} = \boldsymbol{\omega}_{F,a}$
case $\boldsymbol{R}_{SB}$: $\boldsymbol{u}_{F} = \boldsymbol{u}_{F,a}, \boldsymbol{\omega}_{F} = \mathbf{0}$
default: $\boldsymbol{u}_{F} = \boldsymbol{u}_{F,p}, \boldsymbol{\omega}_{F} = \boldsymbol{\omega}_{F,p}$
end switch

3.4 Methodology for the Implementation of Control Strategy

This section describes the methodology used to implement the control strategy of reference [1]. First of all, it is important to clarify that all simulation studies conducted in MATLAB environment.

Initially, it is necessary to simulate the kinematic model of each robot which is described in (2.4). Apparently, the kinematic model consists of a system of non-linear, nonstiff, ordinary, differential equations which has the following form:

$$\dot{y} = f(t, y) \tag{3.37}$$

This system includes the position p_i, the orientation θ_i and the control inputs u_i and ω_i of each robot. Thus, a function was created in MATLAB to define the system. The inputs of the function are the scalar quantity which is the time and the vector quantities which are

the position p_i and the orientation θ_i of each robot. In this function, the control input commands are calculated. If the leader tracking objective is given top priority, the control inputs u_i and ω_i are calculated from equations (3.5) and (3.6). However, if multiregional obstacle avoidance algorithm is activated, the control inputs are calculated based on the strategy which is presented in Table 1 and a combination of equations (3.5), (3.6), (3.20) and (3.21). Moreover, the strategy which is described in Table 2 and equations (3.20), (3.21), (3.31) and (3.32) are used for the calculation of control input commands if leader-loss situation occurs.

To solve the aforementioned system, the solver ode45 from the MATLAB library was used. The function ode45 is based on Runge-Kutta method. In ode45 for the calculation of $y(t_n)$ is only necessary the solution of the previous step $y(t_{n-1})$. Generally, ode45 is an appropriate solver for nonstiff problems. The inputs of ode45 are the function which describes the robots' kinematic model, the time span where the integrator solves the system of differential equations and the vector of initial conditions. For each successful step in time span the integrator returns the calculated solution. The output of ode45 consists of one vector and a numerical matrix. The vector includes the times in which the integrator has calculated the solutions and the numerical matrix consists of the system's solutions i.e. the position p_i and the orientation θ_i of each robot corresponding to the values of vector.

4. Results

To validate the effectiveness of the proposed control algorithms three simulation studies conducted in MATLAB environment.

4.1 Simulation Study A

Firstly, in this particular simulation study, two robots, one leader and one follower, operate in environment with many polygonal obstacles. The obstacle environment and the robot paths are depicted in Figure 7. The robot named *L* moves autonomously in the workspace under the following trajectory.

$$\omega(t) = 0.09\sin(0.05t) \tag{4.1}$$

At the same time, *F* tracks *L* and performs obstacle and interrobot collision avoidance. The kinematic model of robots is given as follows:

$$\dot{x}_L = u_L cos\theta_L$$

$$\dot{y}_L = u_L sin\theta_L$$

$$\dot{\theta}_L = 0.09\sin(0.05t)$$

$$\dot{x}_F = u_F cos\theta_F$$

$$\dot{y}_F = u_F sin\theta_F$$

$$\dot{\theta}_F = \omega_F$$

The initial position and orientation of two robots are presented as follows:

$$p_{L,initial} = [0,0]^T$$

$$p_{F,initial} = [-1,-1]^T$$

$$\theta_{L,initial} = \frac{\pi}{4}$$

$$\theta_{F,initial} = \frac{\pi}{6}$$

Obviously, at $t = 0$, *L* is within the FOV of *F.* Moreover, the time span of the simulation is set as:

$$t_{span} = [0 \quad 300]$$

The robot paths in Figure 7: Simulation Study A: Workspace & robot paths ensure that leader tracking and unknown obstacle avoidance have achieved. The effectiveness of the

proposed control strategy in this specific workspace is also demonstrated by the following figures.

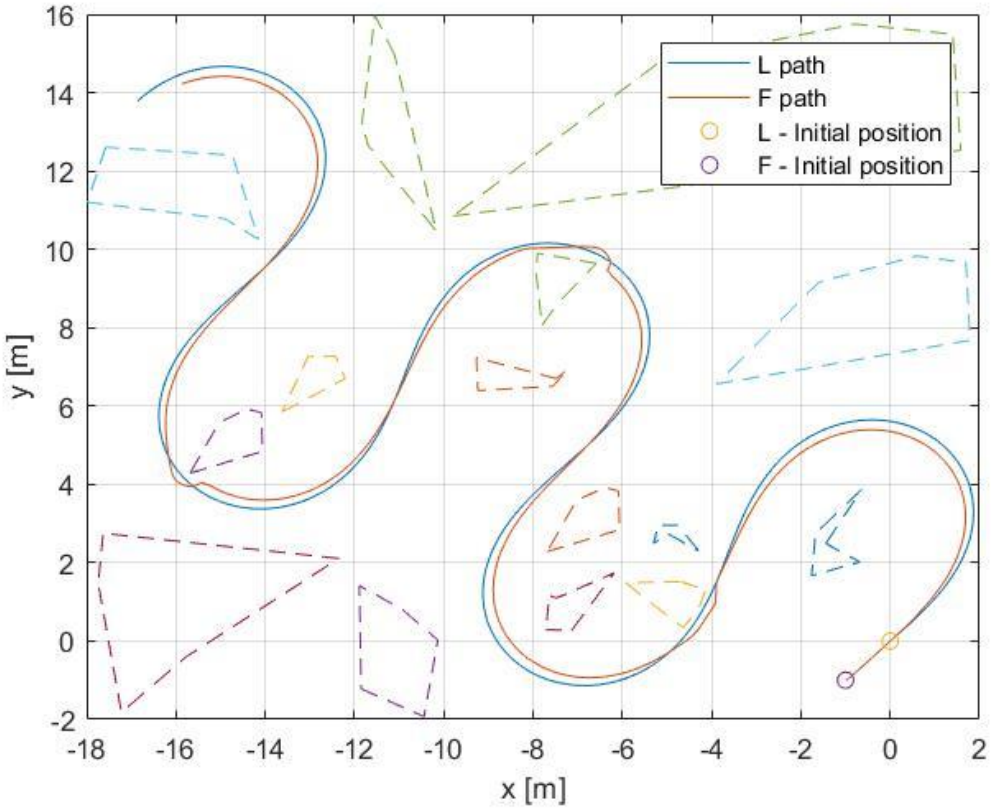

Figure 7: Simulation Study A: Workspace & robot paths

In Table 3 the operational constraints for this simulation study are presented.

Table 3: Simulation Study A: Specifications

ρ_{min}	$0.6\ m$
ρ_{max}	$2.5\ m$
α_{min}	-35°
α_{max}	35°
ρ_d	$1\ m$
α_d	0°
$\rho_{o,safe}$	$0.3\ m$

Next, Table 4 shows the control parameters that have been selected for leader tracking. It is important to mention that these parameters satisfy the constraints (3.7) and (3.8).

Table 4: Simulation Study A: Control parameters for leader tracking

$\bar{u}_L$	$0.3\ m/s$
$\bar{u}_F$	$0.8\ m/s$
$\bar{\omega}_L$	$2\ rad/s$
$\bar{\omega}_F$	$2\ rad/s$
β_ρ	10
β_α	1
k_ρ	0.0068
k_α	0.39
δ_ρ	0.35
δ_α	0.1

Moreover, the parameters of the control protocol for unknown obstacle avoidance were chosen based on constraints (3.18), (3.22) and (3.23) and are given in Table 5.

Table 5: Simulation Study A: Control parameters for unknown obstacle avoidance

$\rho_{o,sen}$	$0.5\ m$
β_{ao}	1
k_{ao}	1
α_{od}	120°
u_{avoid}	$0.3\ m/s$

Furthermore, the control parameters for leader-loss situation have been selected in order to satisfy the constraints (3.35) and (3.36) and are presented in Table 6 .

Table 6: Simulation Study A: Control parameters for leader-loss reaction

k_1	1
k_2	1
γ	1
u_{follow}	$0.3\ m/s$
θ_δ	$\pi/2$
β_δ	1

Additionally, in Figure 8 is shown the evolution of distance ρ between *L* and *F*. It is important to notice that ρ is kept near to the desired distance ρ_d throughout the simulation except for three times that presents instantaneous peaks.

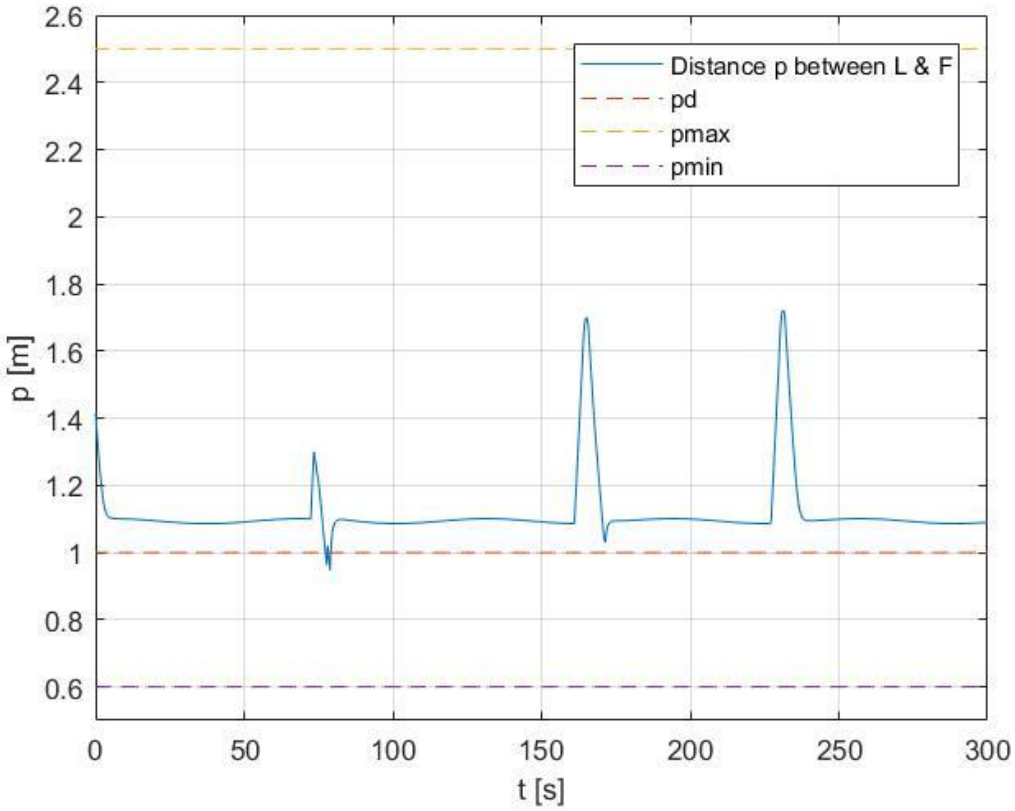

Figure 8: Simulation Study A: Distance *ρ* between *L* & *F* with respect to {*F*}

Apart from that, in Figure 9 the evolution of bearing angle α of *L* with respect to {*F*} is presented. Similar to Figure 8 α almost converges to the desired bearing angle α_d during the whole simulation except for three times that presents pears. Apparently these peaks correspond to the peaks of Figure 8. However, in this case the values of bearing angle α at two of the three peaks are not within the FOV as shown in Figure 9. Therefore, visibility of *L* is lost due to occlusion by an obstacle and leader-loss reaction algorithm is activated with the result that *F* finds *L* and achieves obstacle avoidance simultaneously. Thus, the effectiveness of leader-loss reaction algorithm is demonstrated in Figure 9.

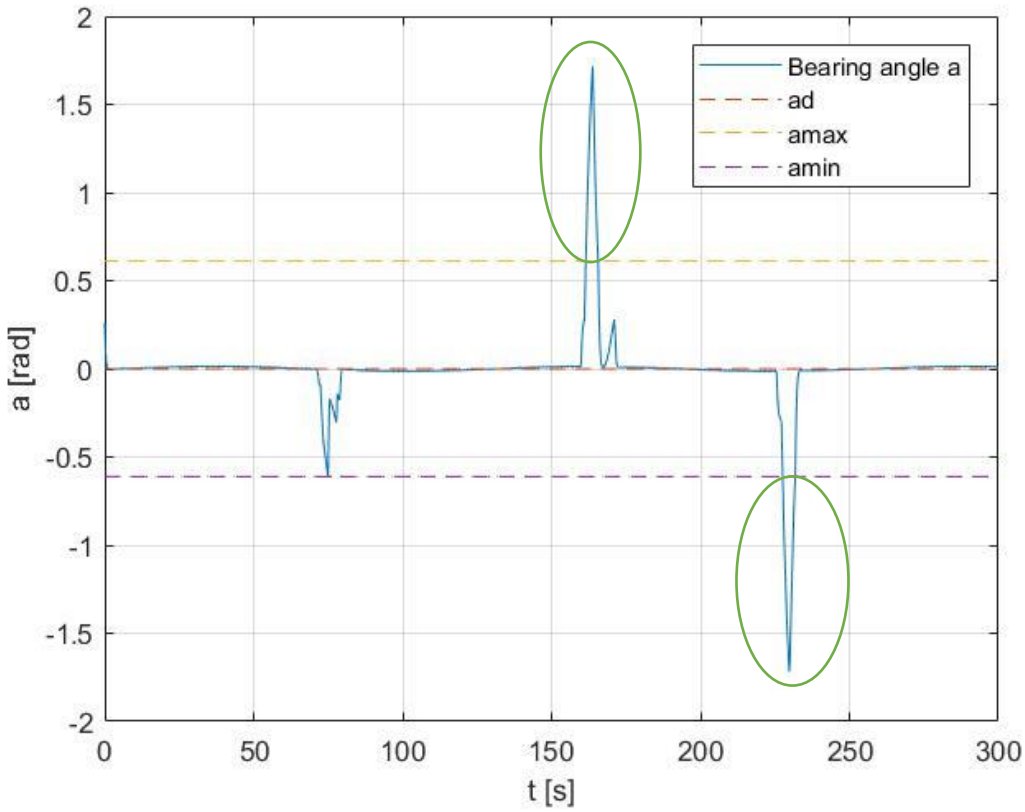

Figure 9: Simulation Study A: Bearing angle *α* of *L* with respect to {*F*}. The marking parts of the curve show the two peaks exceeding the FOV limits indicate the activation of fault-tolerant strategy.

Next, in Figure 10 is presented the evolution of the linear velocity commands for *F*. It should be pointed out that the input linear velocity satisfy the constraint (2.16) and does not exceed the predefined bound $\bar{u}_F$. Moreover, in this particular workspace the linear velocity follows an almost repeated pattern.

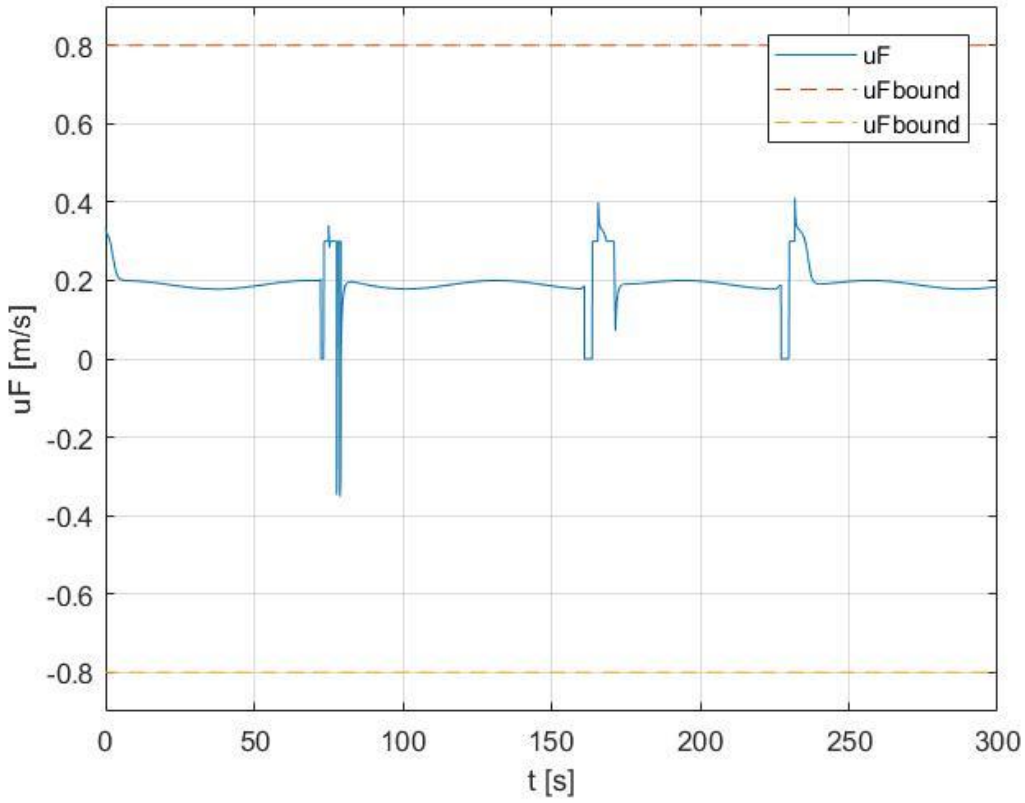

Figure 10: Simulation Study A: Linear velocity of control input

Furthermore, Figure 11 shows the evolution of angular velocity commands for *F.* Similar to Figure 10 the constraint (2.16) is satisfied. Therefore the angular velocity is within the specific bounds. There also seems to be a pattern in this control input. Correspondingly to Figure 10 it can be concluded that the obstacle avoidance behavior and leader-loss reaction change the linear and angular control input velocities dramatically.

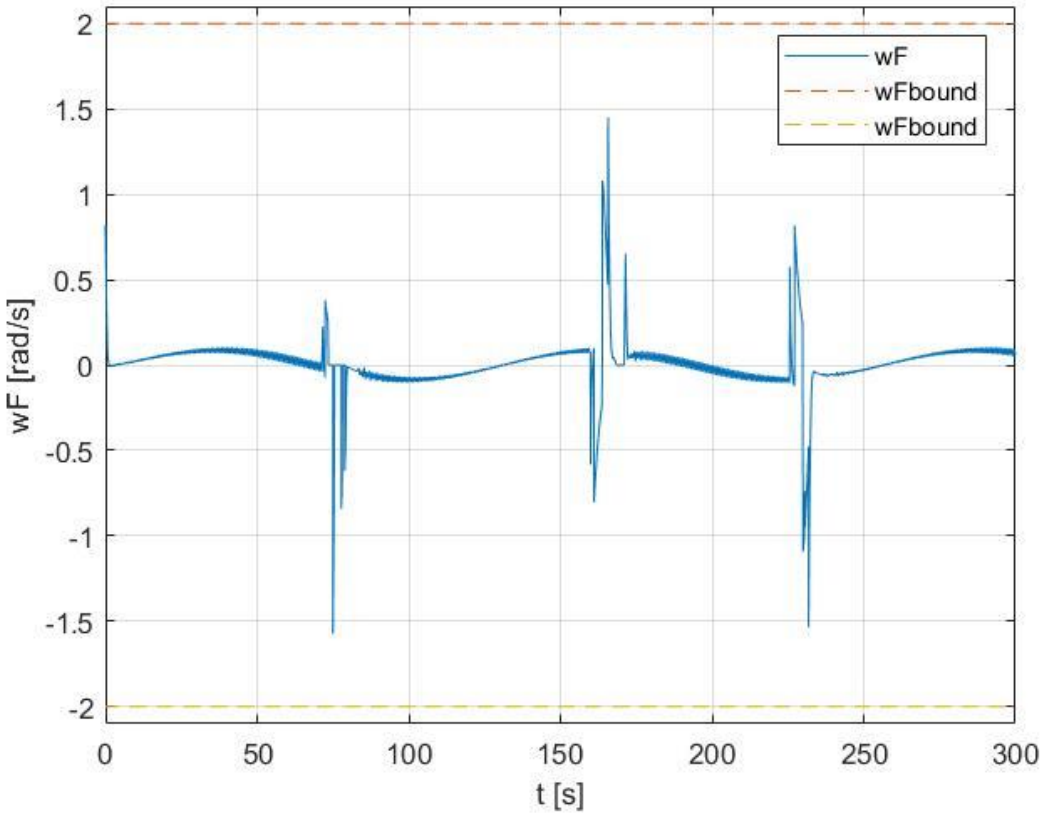

Figure 11: Simulation Study A: Angular velocity of control input

In addition to this, Figure 12 depicts the evolution of minimum distance ρ_o between *F* and the nearest obstacle. Apparently, obstacle avoidance algorithm is activated when ρ_o is smaller than $\rho_{o,sen}$. At about 75 s and 170 s, ρ_o was instantaneously a little smaller than $\rho_{o,safe}$ and obstacle was located in region R_{SF} or region R_{SB}. Therefore, obstacle avoidance objective was prioritized and *F* managed to avoid the obstacle with the appropriate control input velocities. The effectiveness of the proposed control strategy is demonstrated in this figure because *F* succeeded in avoiding all obstacles.

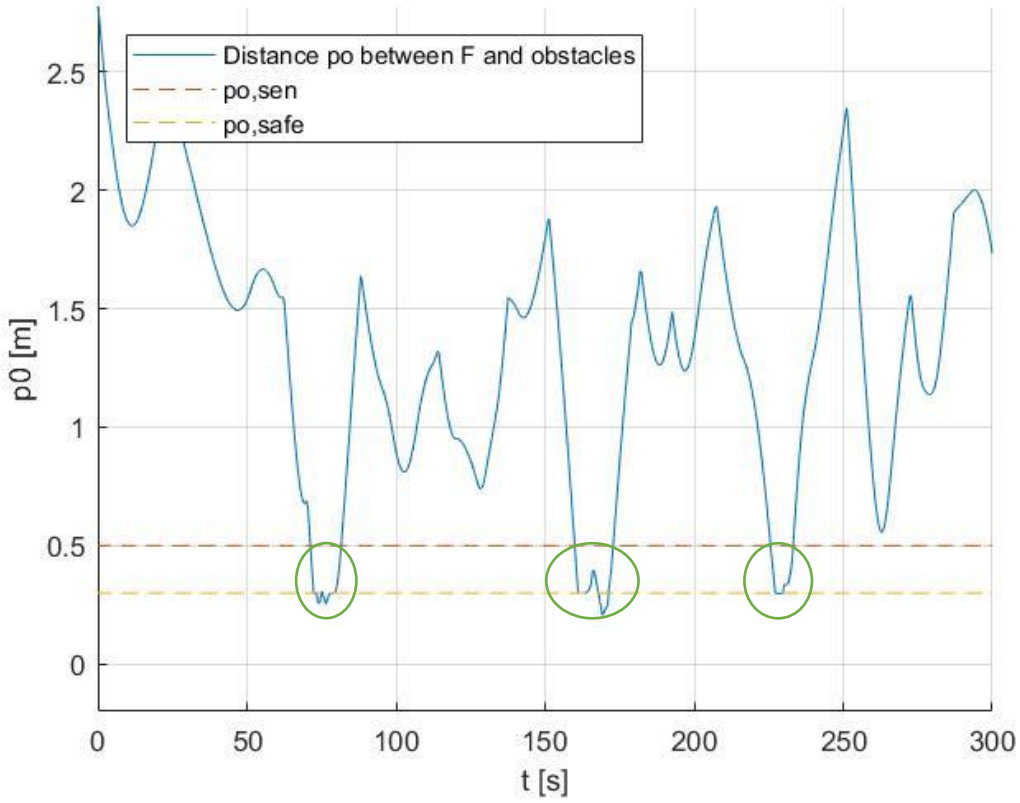

Figure 12: Simulation Study A: Minimum distance between *F* and obstacles. The marking parts of the curve indicate the activation of multiregional obstacle avoidance algorithm.

In Figure 13 is described the evolution of bearing angle α_o of the nearest obstacle with respect to {*F*}. The obstacle avoidance behavior causes the dramatic changes of α_o, especially when obstacle is located in region R_{SF}.

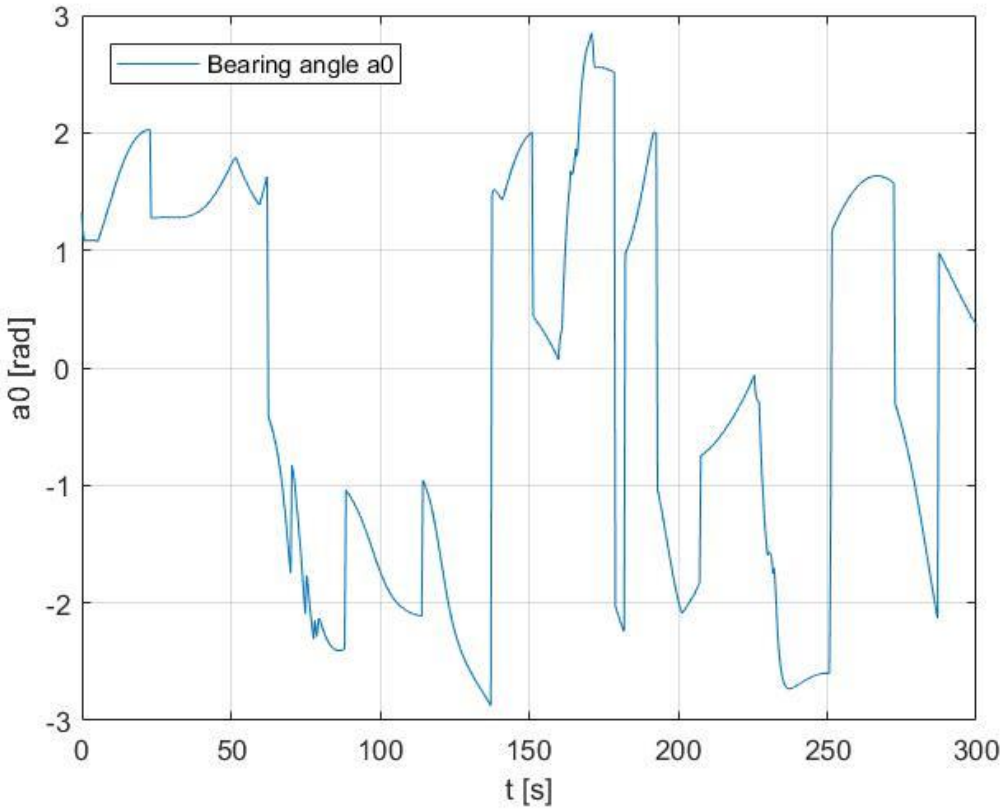

Figure 13: Simulation Study A: Bearing angle of the nearest obstacle measured in {*F*}.

4.2 Simulation Study B

In the second simulation study, a MRS consists of four robots; two followers named F_1 and F_2, as well as one leader named *L*, operating in a workspace with three rooms and many unknown obstacles. *L* moves autonomously from a room to another room though a narrow passage. Because in this case there are two followers, the specific MRS operates as snakelike formation. Therefore F_1 is responsible to track *L* and perform obstacle and interrobot collision avoidance simultaneously. Similar to F_1, F_2 tracks F_1 and avoids the collision with obstacles and with F_1.The objective of this simulation study is to validate the effectiveness of the proposed control strategy in case of multiple followers in a demanding workspace. The trajectory of *L* is given and the method of linear interpolation was used to specify the coordinates of *L* with respect to {*F*}. Apparently, at $t = 0$, *L* is within the FOV of F_1 and F_1 is within the FOV of F_2. The kinematic model of robots is given as follows:

$$\dot{x}_{F_1} = u_{F_1} cos\theta_{F_1}$$

$$\dot{y}_{F_1} = u_{F_1} sin\theta_{F_1}$$

$$\dot{\theta}_{F_1} = \omega_{F_1}$$

$$\dot{x}_{F_2} = u_{F_2} cos\theta_{F_2}$$

$$\dot{y}_{F_2} = u_{F_2} sin\theta_{F_2}$$

$$\dot{\theta}_{F_2} = \omega_{F_2}$$

Moreover, the initial position and orientation of L, F_1 and F_2 are presented as follows:

$$p_{L,initial} = [4, 0.8]^T$$

$$p_{F_1,initial} = [2.5, 0.8]^T$$

$$p_{F_2,initial} = [1, 0.8]^T$$

$$\theta_{L,initial} = 0^\circ$$

$$\theta_{F_1,initial} = 0^\circ$$

$$\theta_{F_2,initial} = 0^\circ$$

Furthermore, the time span of the simulation is set as:

$$t_{span} = [0 \quad 68.5990]$$

The robot paths and the workspace are depicted in Figure 14. It seems that leader tracking and obstacle avoidance were accomplished. The effectiveness of the proposed control scheme is also demonstrated in following figures.

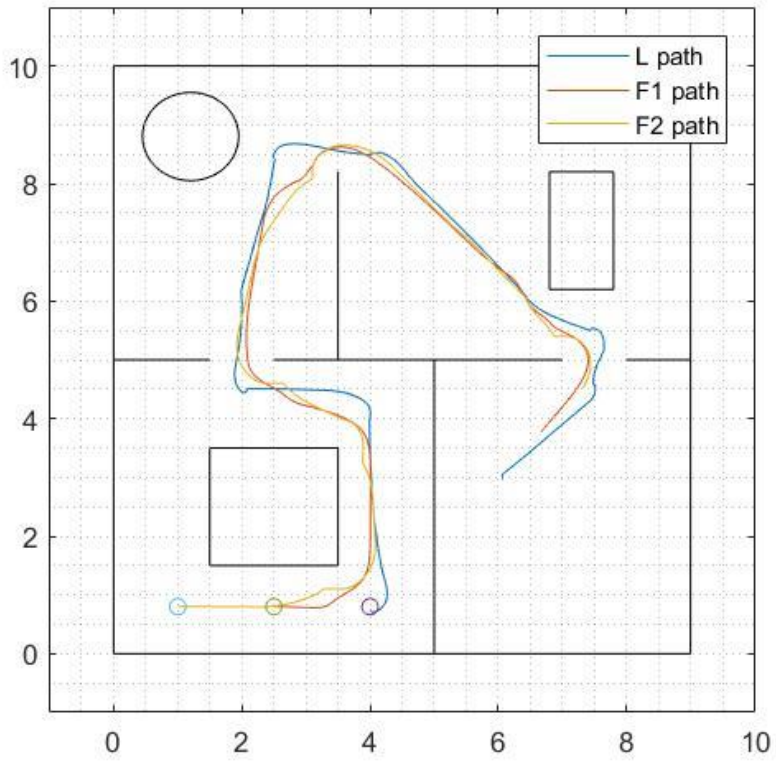

Figure 14: Simulation Study B: Workspace & robot paths

In Table 7 are given the operational constraints for this simulation study. The safe distance $\rho_{o,safe}$ between *F* and obstacles is determined based on the value of robot radius. Obviously, $\rho_{o,safe}$ should be greater than robot radius.

Table 7: Simulation Study B: Specifications

ρ_{min}	$0.6\ m$
ρ_{max}	$2.5\ m$
α_{min}	-45°
α_{max}	45°
ρ_d	$1\ m$
α_d	0°
$\rho_{o,safe}$	$0.4\ m$
$robot\ radius$	$0.3\ m$

Next, Table 8 shows the control parameters that have been selected for leader tracking. The constraints (3.7) and (3.8) should be satisfied separately for F_1 and F_2. Thus, some of the parameters have different value for each follower. Moreover, $\bar{u}_{F_1}$ must be greater than $\bar{u}_L$ and $\bar{u}_{F_2}$ must be greater than $\bar{u}_{F_1}$; otherwise F_1 cannot catch up with *L* and F_2 cannot catch up with F_1. Therefore, provided that the bounds of linear velocity are different for F_1 and F_2, the control parameters will also differ.

Table 8: Simulation Study B: Control parameters for leader tracking

$\bar{u}_L$	$0.3\ m/s$
$\bar{u}_{F_1}$	$0.8\ m/s$
$\bar{u}_{F_2}$	$1.3\ m/s$
$\bar{\omega}_L$	$2\ rad/s$
$\bar{\omega}_{F_1}$	$2\ rad/s$
$\bar{\omega}_{F_2}$	$2\ rad/s$
β_ρ	10
β_α	1
$k_{\rho_{F_1}}$	0.0053
$k_{\rho_{F_2}}$	0.0024
k_α	0.25
δ_ρ	0.35
δ_α	0.1

Moreover, the parameters of the control protocol for unknown obstacle avoidance were chosen based on constraints (3.18), (3.22) and (3.23) and are presented in Table 9. Similar to control parameters which described in Table 8, some parameters have different values for F_1 and F_2 for the same aforementioned reasons.

Table 9: Simulation Study B: Control parameters for unknown obstacle avoidance

$\rho_{o,sen}$	$0.6\ m$
β_{ao}	1
$k_{ao_{F_1}}$	2
$k_{ao_{F_2}}$	1
α_{od}	120°
$u_{avoid_{F_1}}$	$0.3\ m/s$
$u_{avoid_{F_2}}$	$0.5\ m/s$

Furthermore, the control parameters for leader-loss situation have been selected in order to satisfy the constraints (3.35) and (3.36) and are given in Table 10. Corresponding to previous parameters, there are some parameters that have different values for F_1 and F_2.

Table 10: Simulation Study B: Control parameters for leader loss reaction

k_1	1
k_2	1
γ	1
$u_{follow_{F_1}}$	$0.3\ m/s$
$u_{follow_{F_2}}$	$0.5\ m/s$
θ_{δ}	$\pi/2$
β_{δ}	1

Additionally, in Figure 15 is shown the evolution of distance ρ between L and F_1. Distance ρ converges to the desired value ρ_d only the last seconds of simulation. However ρ does not exceed the predefined bounds. The diagram also presents some peaks.

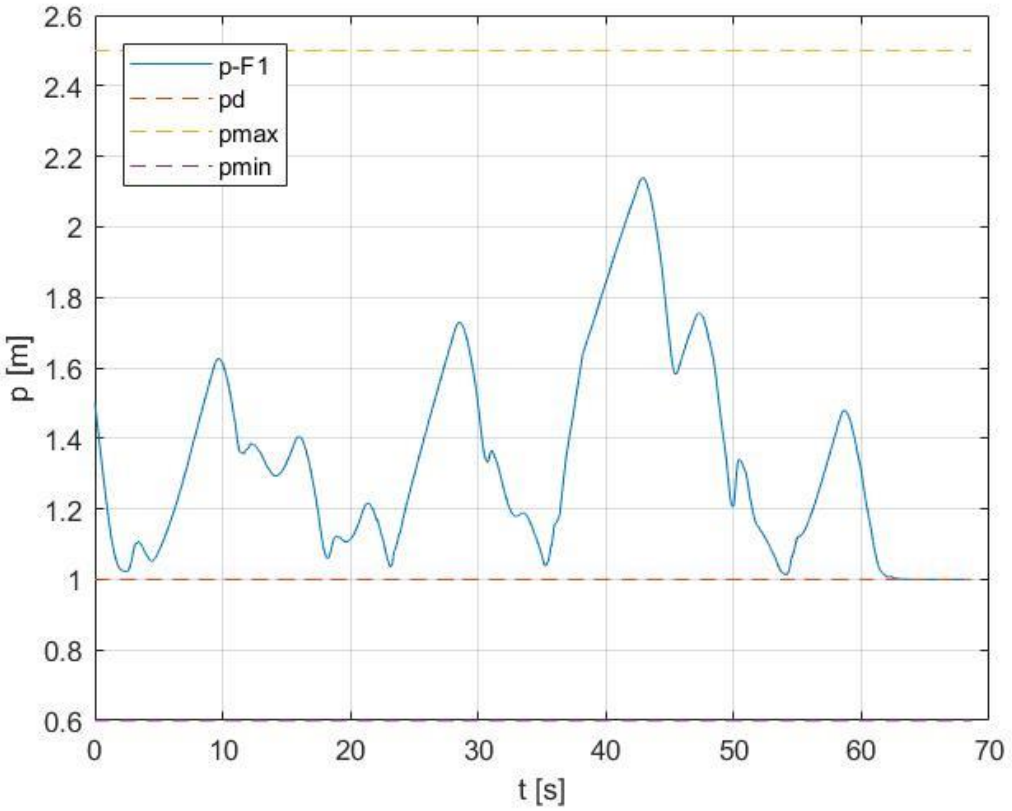

Figure 15: Simulation Study B: Distance ρ between L and F_1 with respect to $\{F_1\}$

Furthermore, Figure 16 depicts the evolution of distance ρ between F_1 and F_2. During the simulation ρ almost converges to the desired distance ρ_d except for six times that presents instantaneous peaks. Nevertheless, these peaks are within the specified limits of the stereo camera.

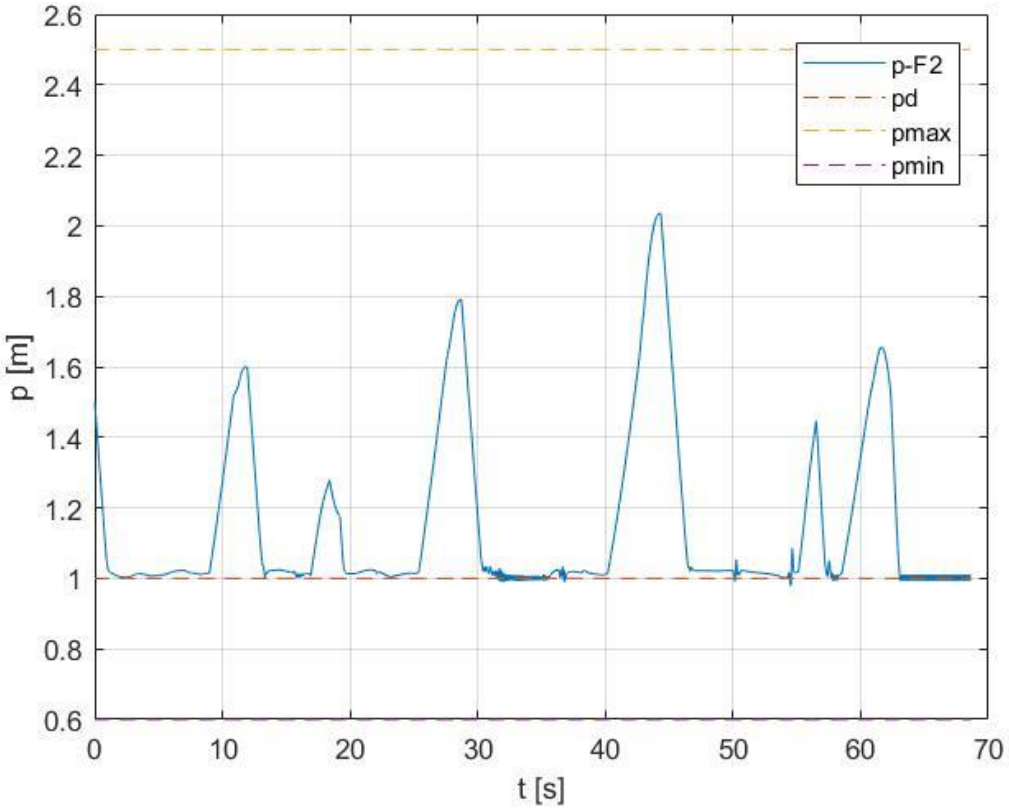

Figure 16: Simulation Study B: Distance ρ between F_1 & F_2 with respect to $\{F_2\}$

In Figure 17 is depicted a comparison between distance ρ between *L* and F_1 and distance ρ between F_1 and F_2. Apparently, distance ρ between F_1 and F_2 is closer to the desired value ρ_d.

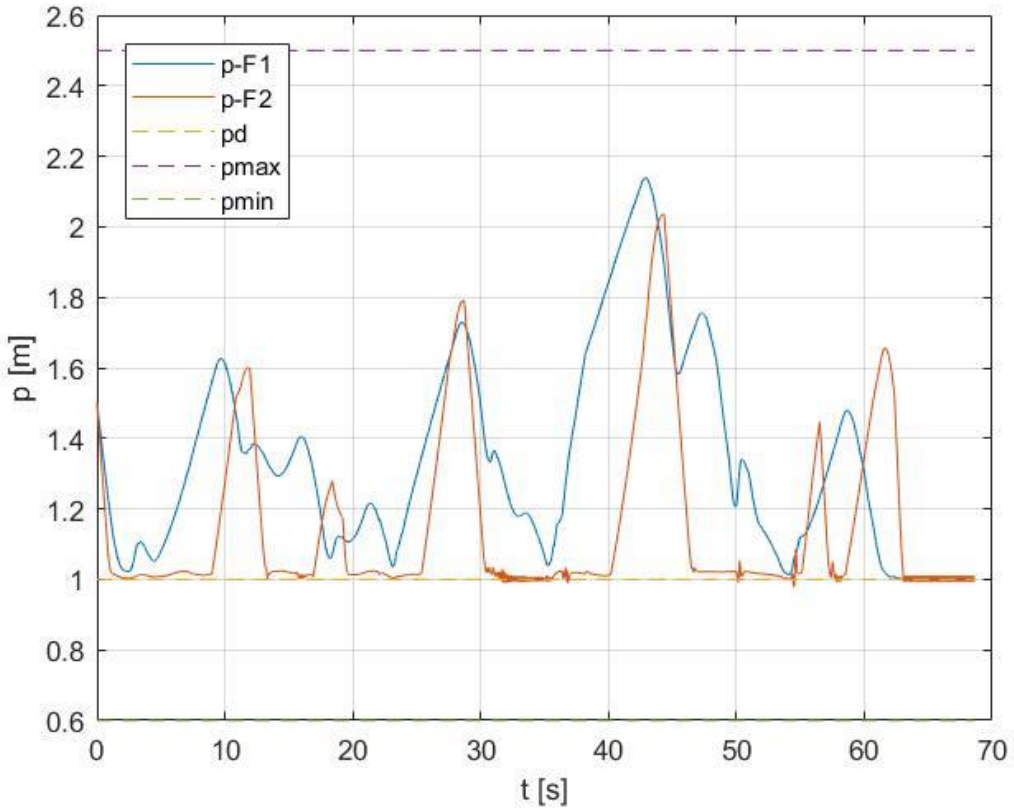

Figure 17: Simulation Study B: Comparison between distance *ρ* between *L* and F_1 and between F_1 & F_2

Additionally, Figure 18 shows the evolution of bearing angle α of L with respect to $\{F_1\}$. As it seems, bearing angle α is close to the desired value α_d except for six times that presents peaks. Five of six peaks are within the FOV. The peak that exceeds the bounds of bearing angle indicates the activation of fault tolerant strategy for leader loss situation. At this particular instant F_1 loses its visual connectivity with *L.* However, with the appropriate control input commands F_1 regains the visibility with *L* again. Therefore, the effectiveness of the proposed control strategy in this workspace is demonstrated. Furthermore, it is important to notice that bearing angle α converges to the desired value α_d the last seconds of simulation.

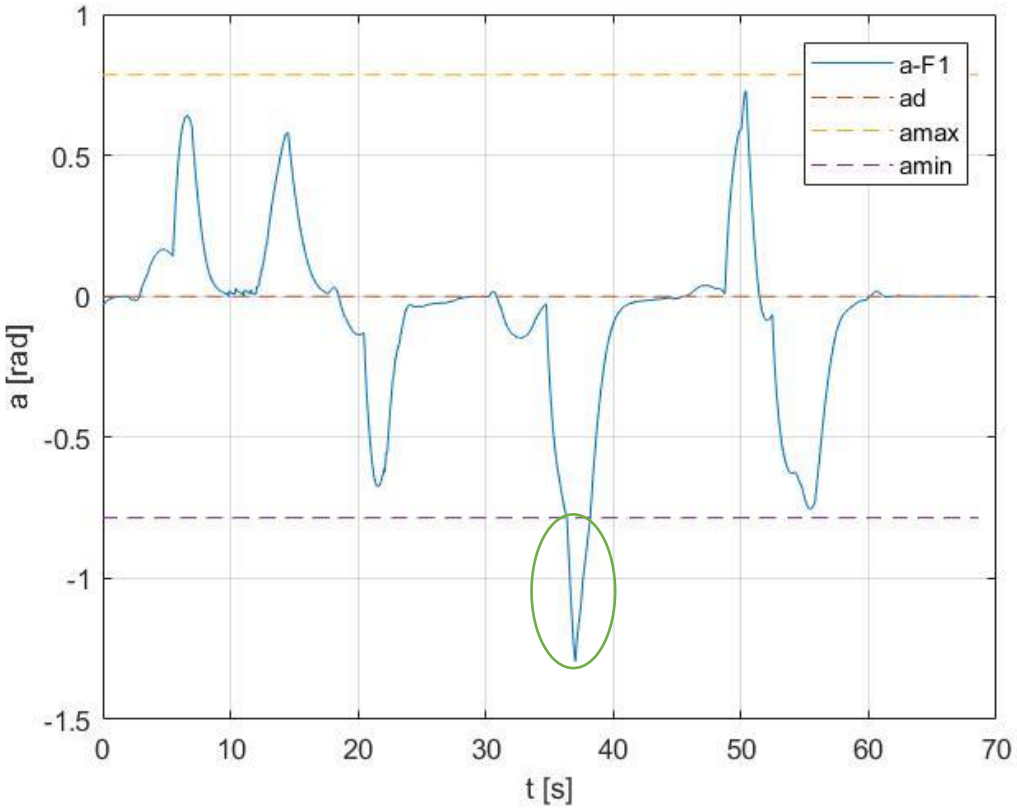

Figure 18: Simulation Study B: Bearing angle α of *L* with respect to $\{F_1\}$. The marking part of the curve shows the peak exceeding the FOV limits and indicates the activation of leader-loss reaction algorithm.

In Figure 19 is depicted the evolution of bearing angle α of F_1 with respect to $\{F_2\}$. Bearing angle α almost converges to the desired value α_d throughout the simulation except for six times that presents instantaneous peak. Five of six peaks are exceeded the predefined limits of FOV. At these instants, F_2 cannot detect F_1. Therefore, the fault-tolerant strategy for leader-loss situation is activated leading F_2 to regain its visual connectivity with F_1.

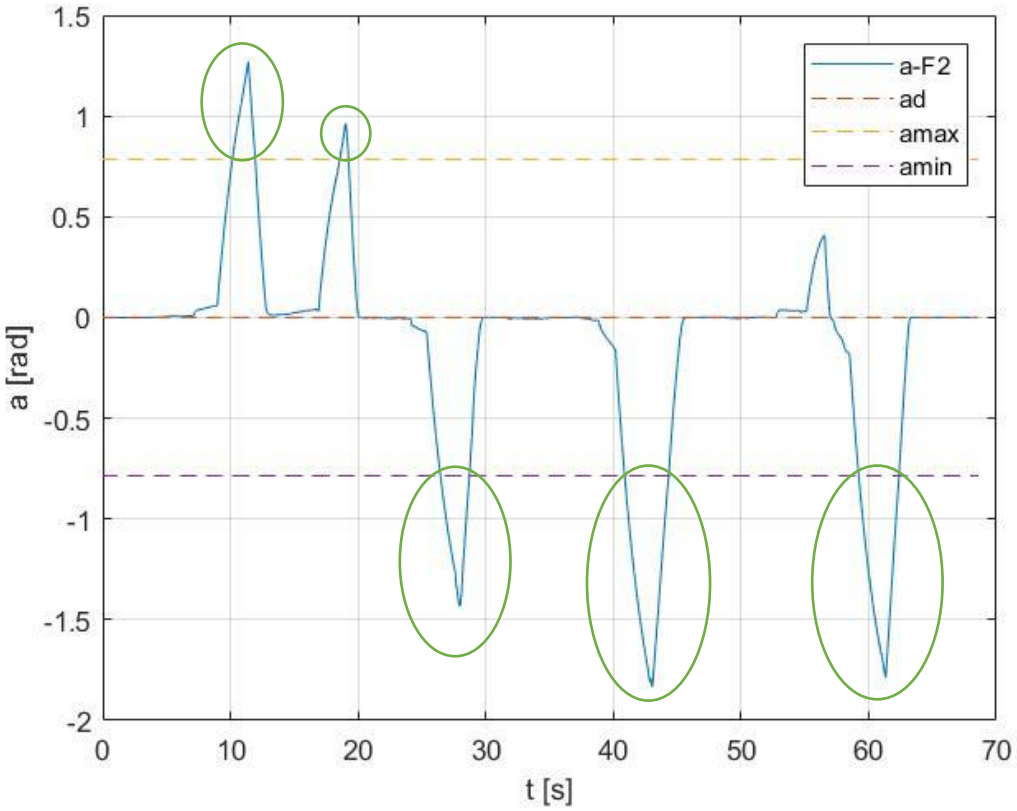

Figure 19: Simulation Study B: Bearing angle α of F_1 with respect to $\{F_2\}$. The marking parts of the curve show the five peaks exceeding the FOV limits and indicate the activation of fault-tolerant strategy.

In Figure 20 is presented the evolution of linear velocity command for F_1. From this figure it can be concluded that control input constraints are satisfied. The dramatic changes of linear velocity are due to obstacle avoidance behavior and leader-loss reaction.

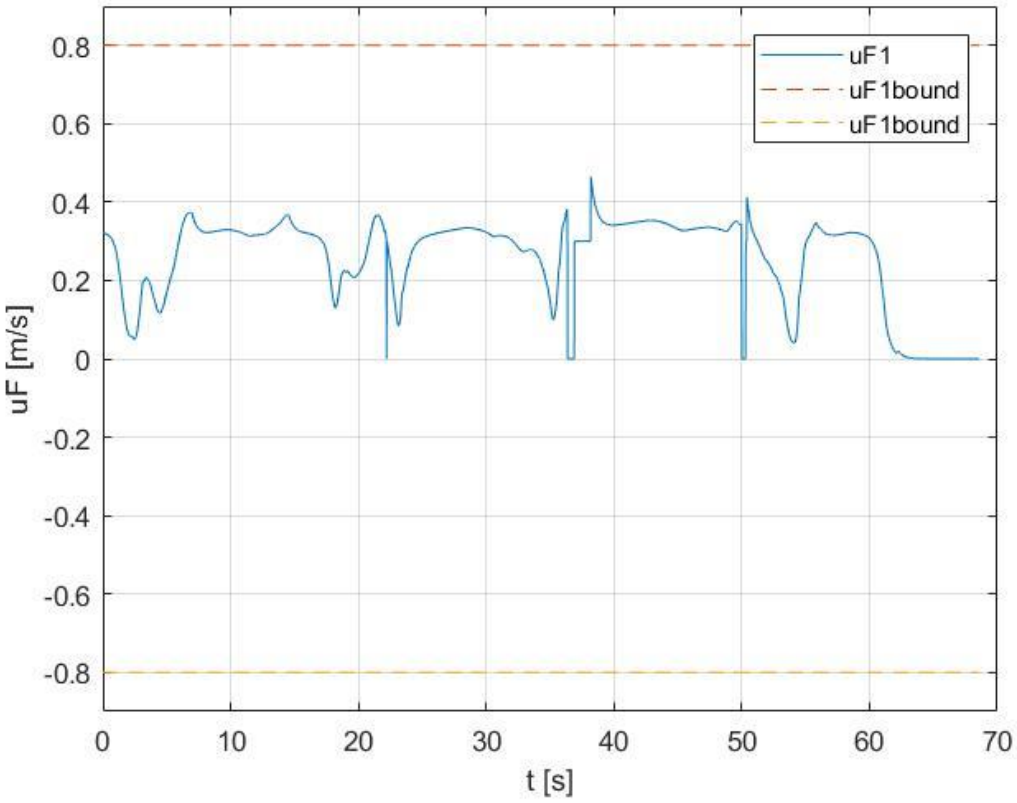

Figure 20: Simulation Study B: Linear velocity of control input for F_1

Moreover, Figure 21 presents the evolution of linear velocity command for F_2. Similar to Figure 20 it can be found that the control input constraints which are given by (2.16) are satisfied. In addition to this, it seems that the linear velocity of F_2 almost follows a pattern. Obviously, the linear velocity of F_2 presents more dramatic changes than the linear velocity of F_1 which are caused by obstacle avoidance behavior and leader loss reaction.

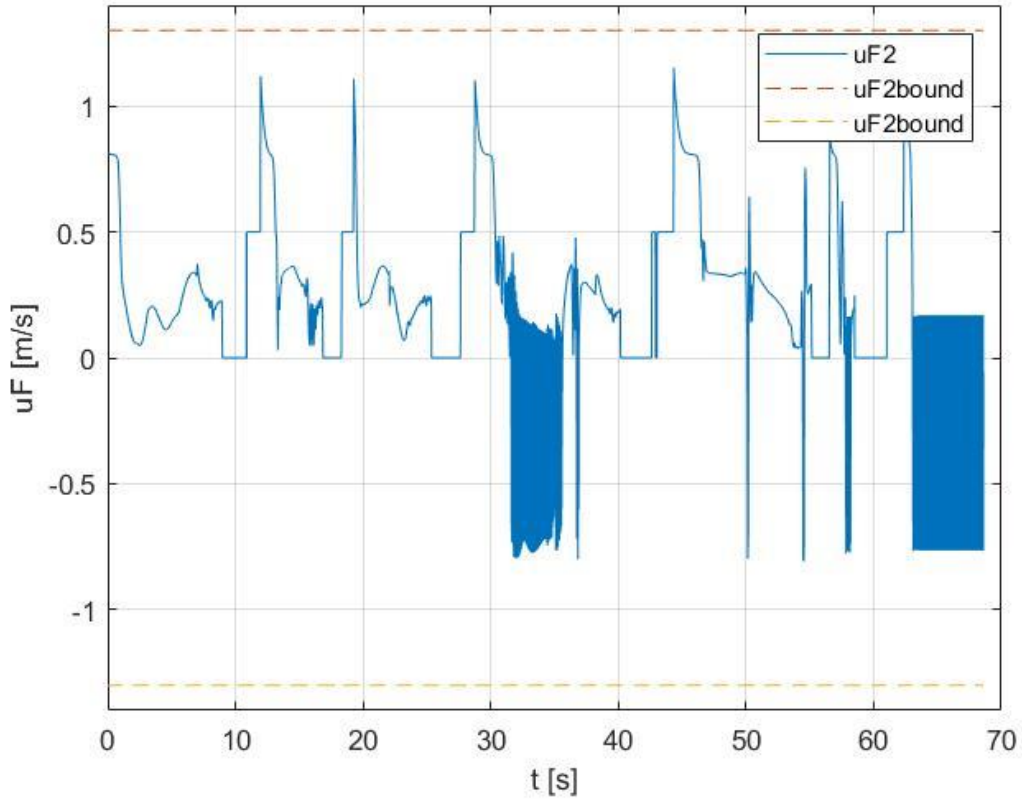

Figure 21: Simulation Study B: Linear velocity of control input for F_2

Furthermore, the evolution of angular velocity command for F_1 is depicted in Figure 22. It is important to notice that the control input bounds are satisfied. Apparently, the angular velocity of F_1 is subject to continuous, abrupt changes throughout the simulation. This behavior is a consequence of obstacle avoidance and leader loss reaction control strategies.

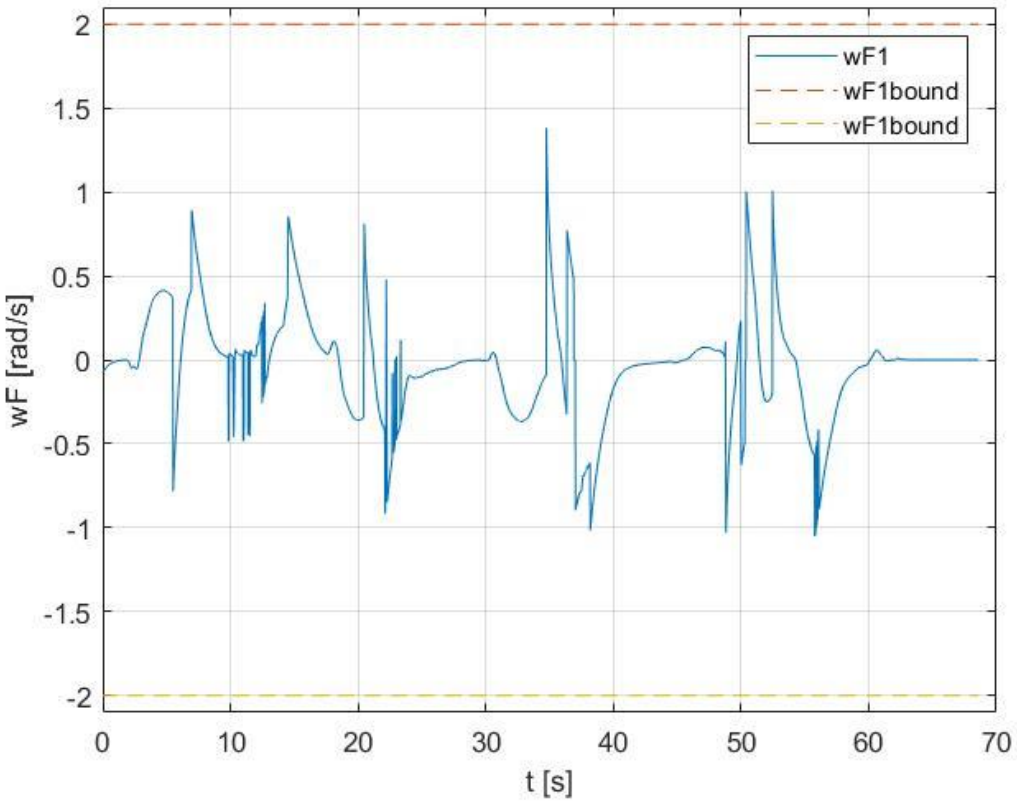

Figure 22: Simulation Study B: Angular velocity of control input for F_1

Next, Figure 23 shows the evolution of angular velocity command for F_2. Similarly with the angular velocity of F_1 in Figure 22, the angular velocity of F_2 satisfy the control input constraints which are given by (2.16) and changes dramatically throughout the simulation for the same aforementioned reasons.

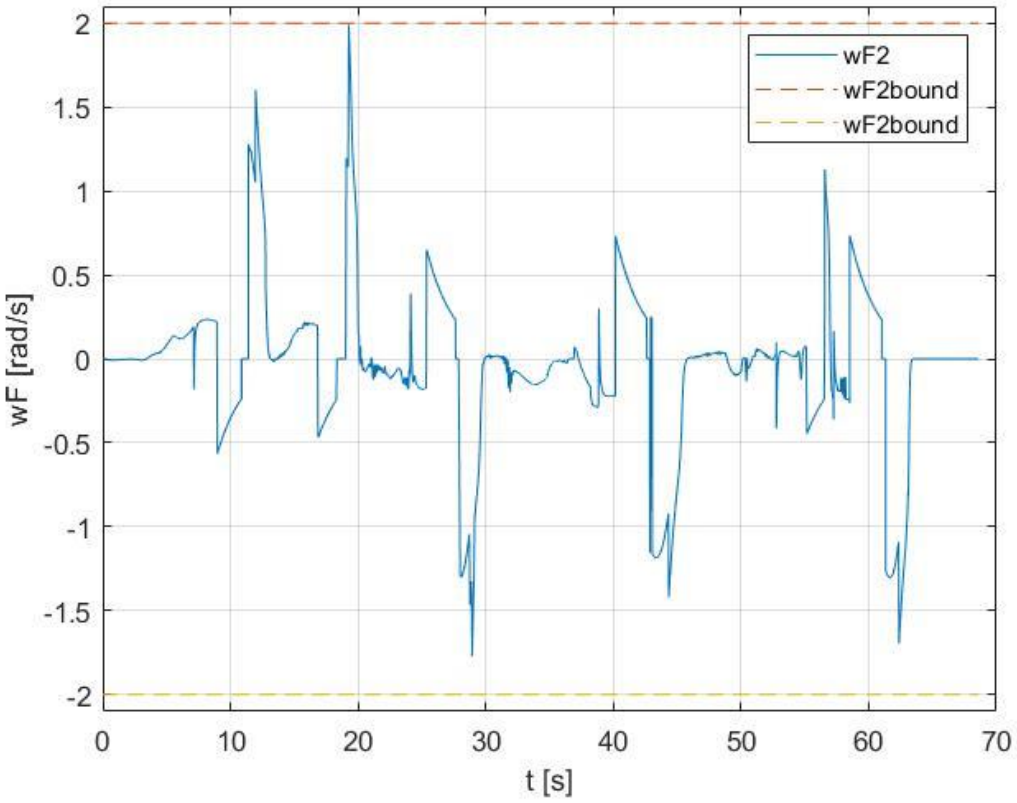

Figure 23: Simulation Study B: Angular velocity of control input for F_2

Apart from that, the evolution of minimum distance ρ_o between F_1 and obstacles is presented in Figure 24. When ρ_o is greater than $\rho_{o,sen}$ the safety of F_1 is not threatened by obstacles and the only objective of the proposed control strategy is leader tracking. However, when ρ_o is between $\rho_{o,sen}$ and $\rho_{o,safe}$ as well as the obstacle is located in front of F_1, i.e. the obstacle is located in region R_{TF}, the proposed control strategy combines the objective of leader tracking or leader loss reaction with obstacle avoidance. Apparently, ρ_o is maintained greater than or equal to $\rho_{o,safe}$ during the whole simulation. Therefore obstacle avoidance for F_1 is achieved.

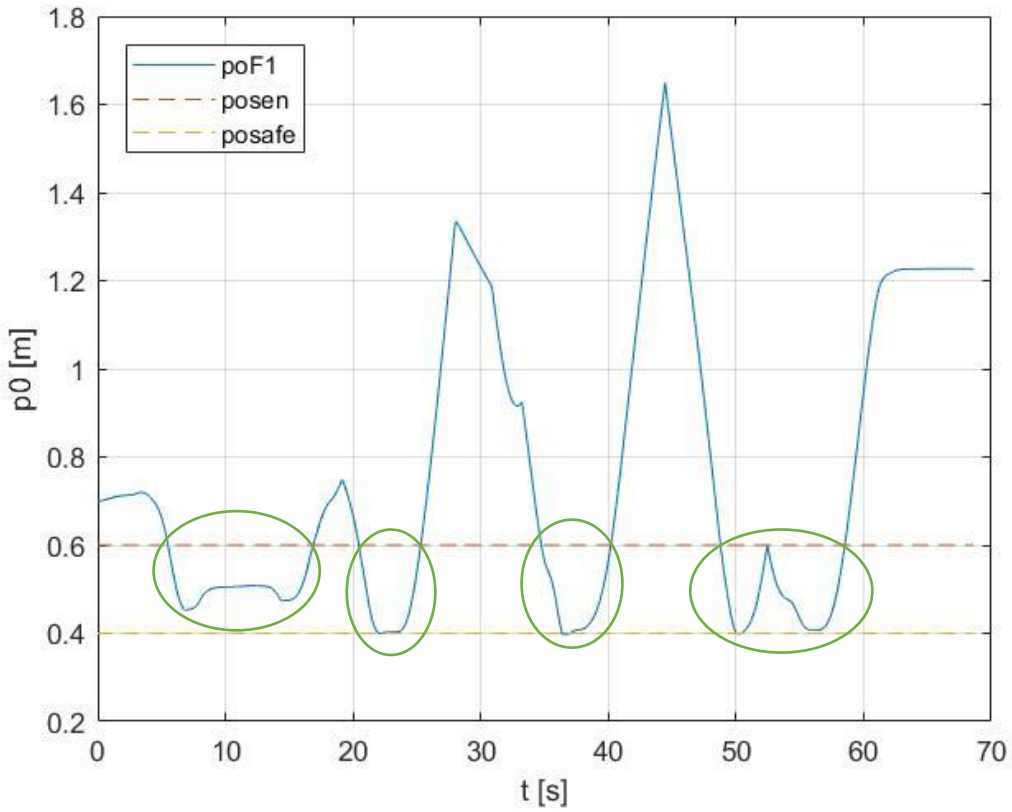

Figure 24: Simulation Study B: Minimum distance between F_1 and obstacles. The marking parts of the curve indicate the activation of obstacle avoidance algorithm.

Continuing with Figure 25 showing the evolution of distance ρ_o between F_2 and the nearest obstacle it is equally important to note that obstacle avoidance is also achieved for F_2. Obviously, ρ_o is maintained equal to or greater than $\rho_{o,safe}$ throughout the simulation except at certain times that is slightly smaller than $\rho_{o,safe}$. From 15 to 20 s the nearest obstacle is located in region R_{SF} or region R_{SB}. Therefore, the obstacle avoidance algorithm is activated by moving F_2 to the appropriate safe distance from the obstacle. Similar to Figure 24, the effectiveness of obstacle avoidance algorithm in this particular workspace is guaranteed.

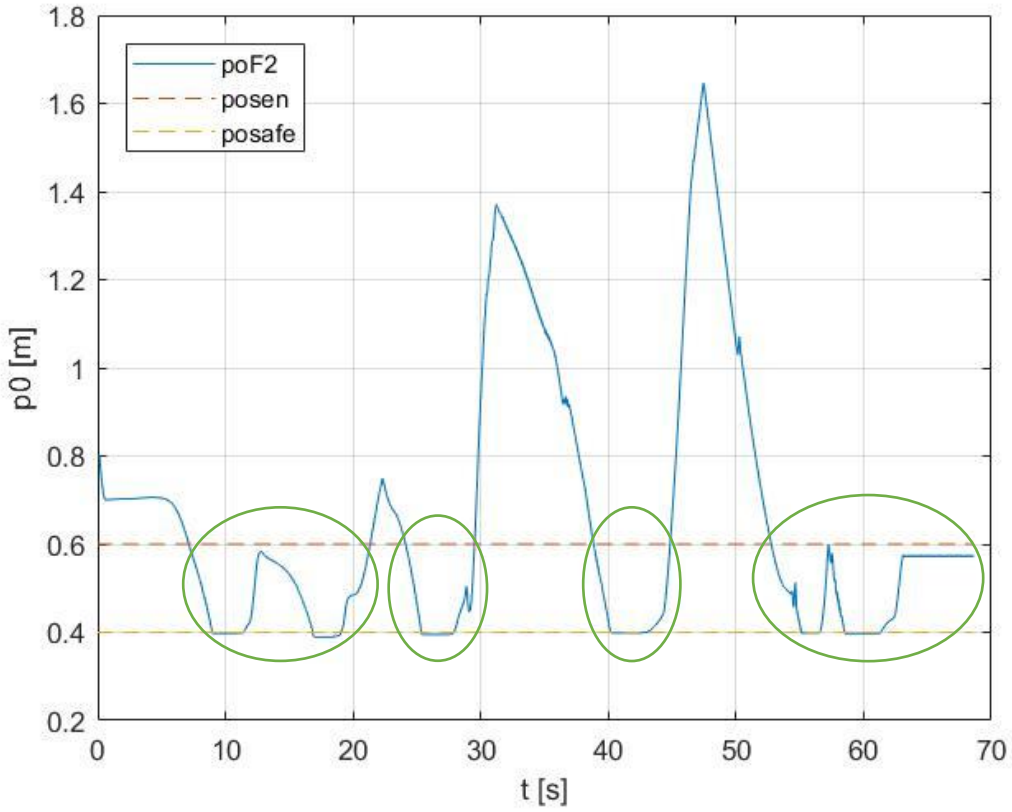

Figure 25: Simulation Study B: Minimum distance between F_2 and obstacles. The marking parts of the curve indicate the activation of multiregional obstacle avoidance algorithm.

Next, Figure 26 describes the evolution of bearing angle α_o of the nearest obstacle measured in $\{F_1\}$. It is important to mention that the obstacle avoidance behavior causes the dramatic changes of α_o, especially when obstacle is located in region R_{SF}.

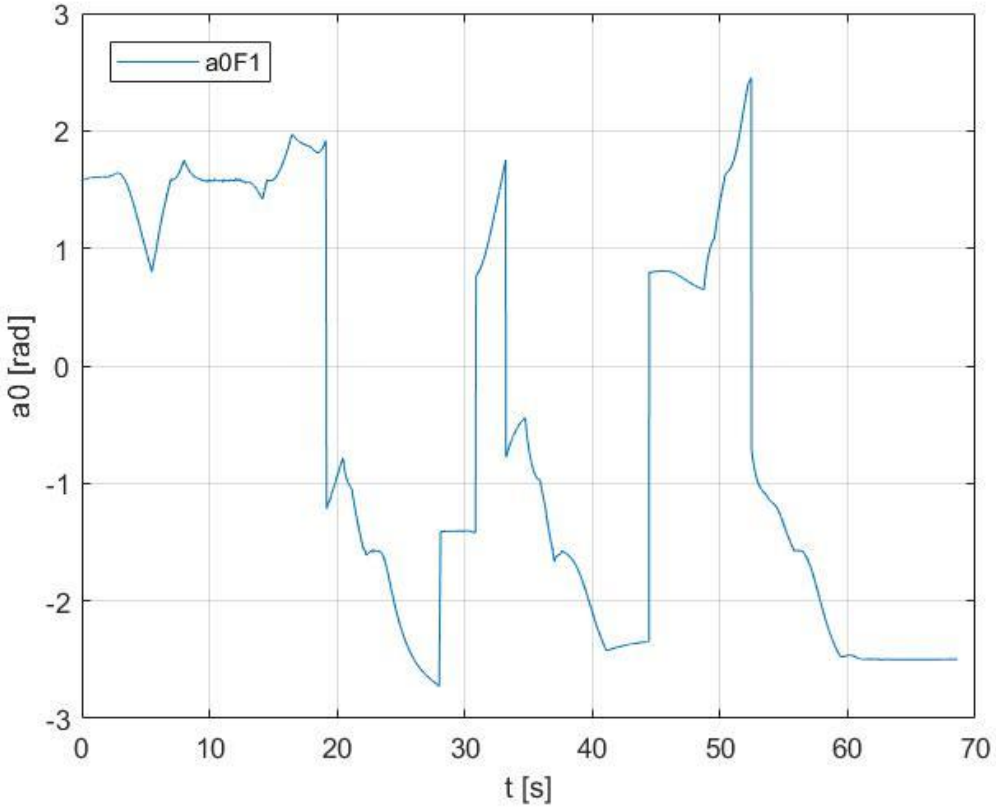

Figure 26: Simulation Study B: Bearing angle α_o of the nearest obstacle measured in $\{F_1\}$

Lastly, in Figure 27 is presented the evolution of bearing angle α_o of the nearest obstacle measured in $\{F_2\}$. The bearing angle α_o measured in $\{F_2\}$ has almost the same pattern as in Figure 26.

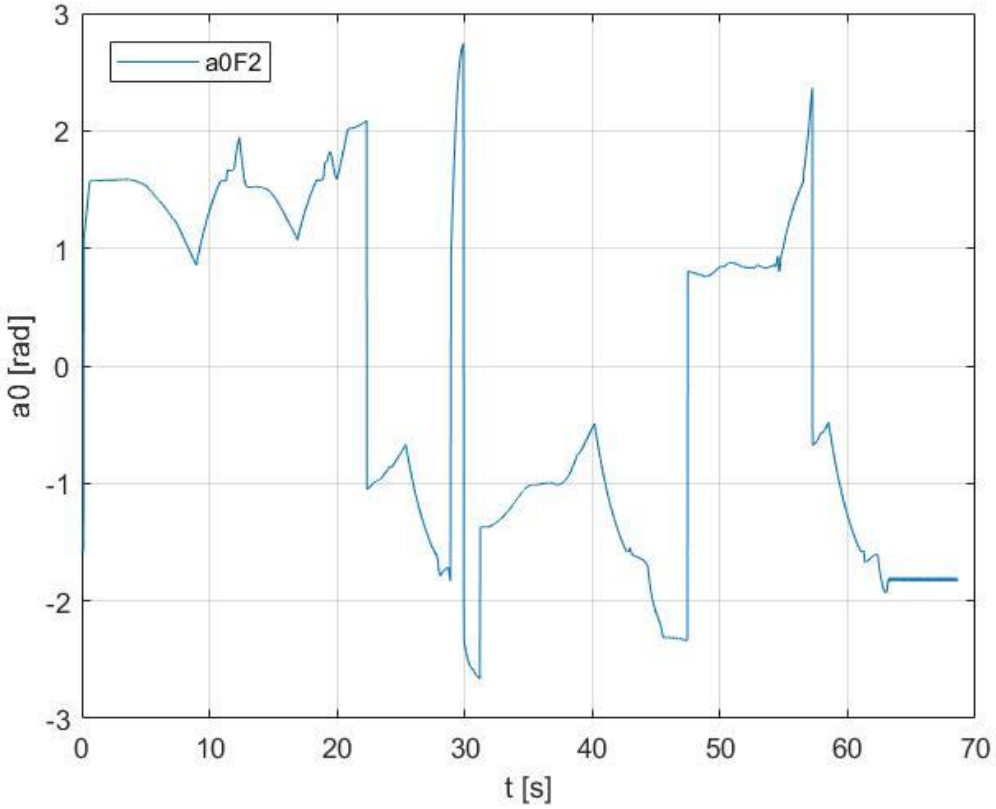

Figure 27: Simulation Study B: Bearing angle α_o of the nearest obstacle measured in $\{F_2\}$

4.3 Simulation Study C

In this case study, two robots; one leading and one following, operate inside a complex workspace which is consisted by a narrow corridor with sharp corners and many non-convex obstacles. The leading robot moves autonomously in the workspace while the following one is responsible to track *L* and avoiding interrobot and obstacle collisions simultaneously. The path of *L* is given and the method of linear interpolation is used to specify the coordinates of *L* with respect to $\{F\}$. Obviously at $t = 0$, *L* is within the FOV of *F.* The objective of this simulation study is to check if the proposed control strategy is effective in a workspace similar to zigzag. The kinematic model of robots is given as follows:

$$\dot{x}_F = u_F cos\theta_F$$

$$\dot{y}_F = u_F sin\theta_F$$

$$\dot{\theta}_F = \omega_F$$

The initial position and orientation of *F* is presented as follows:

$$p_{F,initial} = [0.5, -3.5]^T$$

$$\theta_{F,initial} = 45^\circ$$

Moreover, the duration of simulation is set as:

$$t_{span} = [0 \quad 32.4]$$

The robot paths and the workspace are depicted in Figure 28. Apparently, *F* is able to track *L* until a specific point and then stops. It seems that *F* lost its visual connectivity with *L* at the first corner of the corridor. Therefore, the fault tolerant strategy was activated and thus *F* performed a maneuver towards the position where *L* was last detected. However, in this position *L* was not within the FOV again. As a result *F* was not able to regain its visual connectivity with *L.* This behavior demonstrates the inefficiency of proposed control strategy in workspaces where the visibility of the preceding robot is constantly lost.

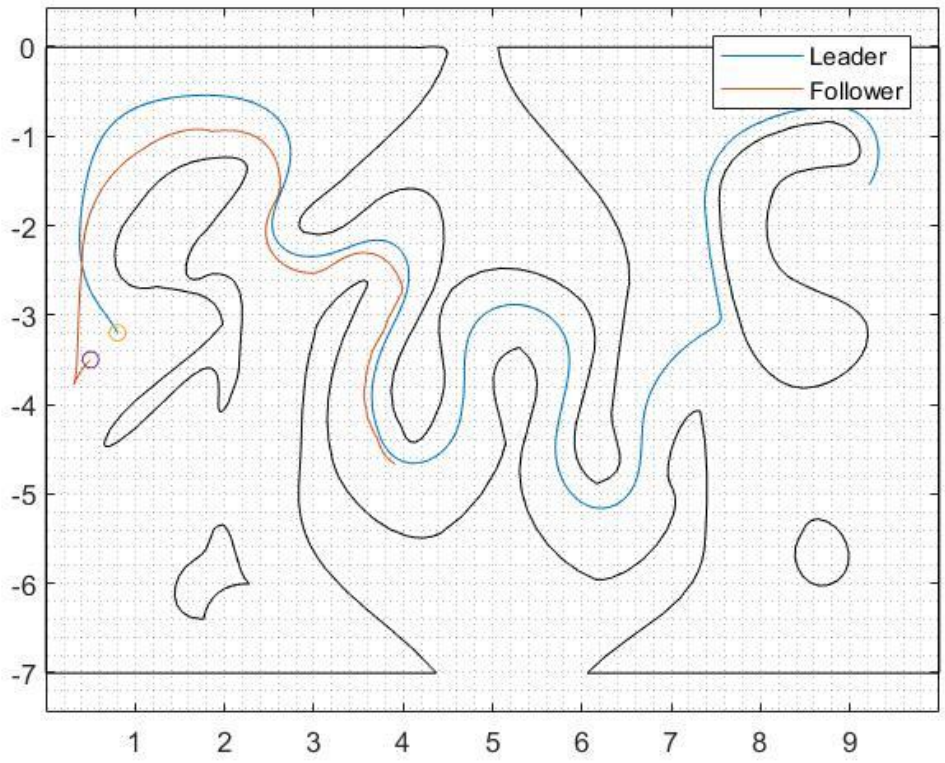

Figure 28: Simulation Study C: Workspace & robot paths

In Table 11 the operational constraints for this simulation study are presented.

Table 11: Simulation study C: Specifications

ρ_{min}	$0.4\ m$
ρ_{max}	$1.5\ m$
α_{min}	$-0.4\ rad$
α_{max}	$0.4\ rad$
ρ_d	$1\ m$
α_d	0°
$\rho_{o,safe}$	$0.3\ m$
$robot\ radius$	$0.15\ m$

Next, Table 12 shows the control parameters that have been selected for leader tracking. It is important to mention that these parameters satisfy the constraints (3.7) and (3.8).

Table 12: Simulation Study C: Control parameters for leader tracking

$\bar{u}_L$	$0.3\ m/s$
$\bar{u}_F$	$1\ m/s$
$\bar{\omega}_L$	$2\ rad/s$
$\bar{\omega}_F$	$2\ rad/s$
β_ρ	10
β_α	1
k_ρ	0.015
k_α	0.3
δ_ρ	0.35
δ_α	0.1

Moreover, the parameters of the control protocol for unknown obstacle avoidance were chosen based on constraints (3.18), (3.22) and (3.23) and are given in Table 13.

Table 13: Simulation Study C: Control parameters for unknown obstacle avoidance

$\rho_{o,sen}$	$0.4\ m$
$\beta_{\alpha o}$	1
k_{ao}	2
α_{od}	120°
u_{avoid}	$0.5\ m/s$

Furthermore, the control parameters for leader-loss situation have been selected in order to satisfy the constraints (3.35) and (3.36) and are presented in Table 14.

Table 14: Simulation Study C: Control parameters for leader loss reaction

k_1	1
k_2	1
γ	1
u_{follow}	$0.3\ m/s$
θ_δ	$\pi/2$
β_δ	1

5. Discussion

In this diploma thesis is investigated the reliability of the control strategy proposed in [1] in many different demanding workspaces.

In Simulation Study A is proven that the proposed control strategy is effective in a workspace with multiple polygonal obstacles. The objectives of leader tracking, obstacle avoidance and leader-loss reaction have been accomplished and control input constraints have been satisfied.

In Simulation Study B the proposed control strategy is applied for three robots operating in a workspace consisting of three rooms and narrow passages. Similar to Simulation Study A, both followers succeeded in avoiding all obstacles despite that fault-tolerant algorithm was activated several times throughout the simulation.

Finally, in Simulation Study C, two robots operate in a workspace similar to zigzag with many non-convex obstacles and sharp corners. In this simulation is has been proven that the proposed control strategy is not able to achieve the leader tracking objective in workspaces where the visibility of the preceding robot is constantly lost.

6. List of Tables

7. List of Figures

8. Bibliography

[1] Y. Wang, D. Wang, S. Yang, and M. Shan, "A Practical Leader-Follower Tracking Control Scheme for Multiple Nonholonomic Mobile Robots in Unknown Obstacle Environments," *IEEE Transactions on Control Systems Technology*, vol. 27, no. 4, pp. 1685–1693, 2019, doi: 10.1109/TCST.2018.2825943.

[2] A. Gautam and S. Mohan, "A review of research in multi-robot systems," in *2012 IEEE 7th International Conference on Industrial and Information Systems (ICIIS)*, Chennai, India, Aug. 2012, pp. 1–5. doi: 10.1109/ICIInfS.2012.6304778.

[3] A. Farinelli, L. Iocchi, and D. Nardi, "Multirobot Systems: A Classification Focused on Coordination," *IEEE Trans. Syst., Man, Cybern. B*, vol. 34, no. 5, pp. 2015–2028, Oct. 2004, doi: 10.1109/TSMCB.2004.832155.

[4] K.-K. Oh, M.-C. Park, and H.-S. Ahn, "A survey of multi-agent formation control," *Automatica*, vol. 53, pp. 424–440, Mar. 2015, doi: 10.1016/j.automatica.2014.10.022.

[5] R. W. Beard, J. Lawton, and F. Y. Hadaegh, "A coordination architecture for spacecraft formation control," *IEEE Trans. Contr. Syst. Technol.*, vol. 9, no. 6, pp. 777–790, Nov. 2001, doi: 10.1109/87.960341.

[6] F. Y. Hadaegh and S. R. Ploen, "A Survey of Spacecraft Formation Flying Guidance and Control (Part 11): Control'," p. 10.

[7] D. Panagou and V. Kumar, "Cooperative visibility maintenance for leader-follower formations in obstacle environments," *IEEE Transactions on Robotics*, vol. 30, no. 4, pp. 831–844, 2014, doi: 10.1109/TRO.2014.2304774.

[8] L. Brinon-Arranz, A. Seuret, and C. Canudas-de-Wit, "Cooperative Control Design for Time-Varying Formations of Multi-Agent Systems," *IEEE Trans. Automat. Contr.*, vol. 59, no. 8, pp. 2283–2288, Aug. 2014, doi: 10.1109/TAC.2014.2303213.

[9] E. J. Rodríguez-Seda, C. Tang, M. W. Spong, and D. M. Stipanović, "Trajectory tracking with collision avoidance for nonholonomic vehicles with acceleration constraints and limited sensing," *The International Journal of Robotics Research*, vol. 33, no. 12, pp. 1569–1592, Oct. 2014, doi: 10.1177/0278364914537130.

[10] M. Deghat, I. Shames, and B. D. O. Anderson, "Safe Autonomous Agent Formation Operations Via Obstacle Collision Avoidance: Safe Autonomous Agent Formation Operations Via Obstacle Collision Avoidance," *Asian Journal of Control*, vol. 17, no. 5, pp. 1473–1483, Sep. 2015, doi: 10.1002/asjc.1005.

[11] S. S. Ge, X. Liu, C.-H. Goh, and L. Xu, “Formation Tracking Control of Multiagents in Constrained Space,” *IEEE Trans. Contr. Syst. Technol.*, vol. 24, no. 3, pp. 992–1003, May 2016, doi: 10.1109/TCST.2015.2472959.

[12] X. Liang, Y.-H. Liu, H. Wang, W. Chen, K. Xing, and T. Liu, “Leader-Following Formation Tracking Control of Mobile Robots Without Direct Position Measurements,” *IEEE Trans. Automat. Contr.*, vol. 61, no. 12, pp. 4131–4137, Dec. 2016, doi: 10.1109/TAC.2016.2547872.

[13] H. Wang, D. Guo, X. Liang, W. Chen, G. Hu, and K. K. Leang, “Adaptive Vision-Based Leader–Follower Formation Control of Mobile Robots,” *IEEE Trans. Ind. Electron.*, vol. 64, no. 4, pp. 2893–2902, Apr. 2017, doi: 10.1109/TIE.2016.2631514.

[14] Y. Wang, D. Wang, and B. C. Ng, “Finite time moving target tracking using nonholonomic vehicles with distance and bearing angle constraints,” in *2017 American Control Conference (ACC)*, Seattle, WA, USA, May 2017, pp. 2962–2967. doi: 10.23919/ACC.2017.7963401.

[15] Y. Wang, D. Wang, and S. Zhu, “Formation tracking of multi-vehicle systems in unknown environments using a multi-region control scheme,” *International Journal of Control*, vol. 90, no. 12, pp. 2760–2771, Dec. 2017, doi: 10.1080/00207179.2016.1265151.

[16] X. Liang, H. Wang, Y.-H. Liu, W. Chen, and T. Liu, “Formation Control of Nonholonomic Mobile Robots Without Position and Velocity Measurements,” *IEEE Transactions on Robotics*, vol. 34, no. 2, pp. 434–446, 2018, doi: 10.1109/TRO.2017.2776304.

[17] D. Sakai, H. Fukushima, and F. Matsuno, “Leader-Follower Navigation in Obstacle Environments while Preserving Connectivity Without Data Transmission,” *IEEE Transactions on Control Systems Technology*, vol. 26, no. 4, pp. 1233–1248, 2018, doi: 10.1109/TCST.2017.2705121.

[18] Z. Yang, S. Zhu, C. Chen, and G. Feng, “Leader-Follower Formation Control of Nonholonomic Mobile Robots with Bearing-Only Measurements,” p. 23.

[19] J. Lin, Z. Miao, H. Zhong, W. Peng, Y. Wang, and R. Fierro, “Adaptive Image-Based Leader-Follower Formation Control of Mobile Robots With Visibility Constraints,” *IEEE TRANSACTIONS ON INDUSTRIAL ELECTRONICS*, p. 10.

[20] M. Wang, Z. Geng, and X. Peng, “Measurement-Based Method for Nonholonomic Mobile Vehicles with Obstacle Avoidance,” p. 20.

[21] Y. Xu, C. Wang, X. Cai, Y. Li, and L. Xu, “Output-feedback formation tracking control of networked nonholonomic multi-robots with connectivity preservation and collision avoidance,” *Neurocomputing*, vol. 414, pp. 267–277, Nov. 2020, doi: 10.1016/j.neucom.2020.07.023.

[22] “Nonholonomic multibody mobile robots: Controllability and motion planning in the presence of obstacles,” p. 35.

[23] S. K. Malu and J. Majumdar, “Kinematics, Localization and Control of Differential Drive Mobile Robot,” p. 9, 2014.

[24] R. Castro, Jm. Alvarez, and J. Martinez, “Robot formation control using backstepping and sliding mode techniques,” in *2009 6th International Conference on Electrical Engineering, Computing Science and Automatic Control (CCE)*, Toluca, Nov. 2009, pp. 1–6. doi: 10.1109/ICEEE.2009.5393430.

[25] “Time optimal path planning for a wheeled mobile robot,” p. 7.

[26] D. Soetanto, L. Lapierre, and A. Pascoal, “Adaptive, non-singular path-following control of dynamic wheeled robots,” in *42nd IEEE International Conference on Decision and Control (IEEE Cat. No.03CH37475)*, Maui, Hawaii, USA, 2003, vol. 2, pp. 1765–1770. doi: 10.1109/CDC.2003.1272868.